Exploring Virus–Host Interactions Through Combined Proteomic Approaches Identifies BANF1 as a New Essential Factor for African Swine Fever Virus

Authors

Juliette Dupré, Katarzyna Magdalena Dolata, Gang Pei, Aidin Molouki, Lynnette C. Goatley, Richard Küchler, Timothy K. Soh, Jens B. Bosse, Aurore Fablet, Mireille Le Dimna, Grégory Karadjian, Edouard Hirchaud, Christopher L. Netherton, Linda K. Dixon, Ana Luisa Reis, Damien Vitour, Marie-Frédérique Le Potier, Axel Karger, and Grégory Caignard

Correspondence

katarzyna.dolata@fli.de; axel.karger@fli.de; gregory.caignard@vet-alfort.fr

In Brief

African swine fever virus (ASFV) causes deadly disease in pigs and threatens pork production worldwide. This study identifies a host protein, BANF1, as crucial for ASFV replication and as a target of two viral proteins, A151R and MGF360-21R. These viral proteins disrupt immune defenses by inhibiting the interferon signaling. Removing them from the virus enhances the host immune response. This work reveals how ASFV manipulates host cells and highlights BANF1 as a potential target for future antiviral strategies.

Graphical Abstract

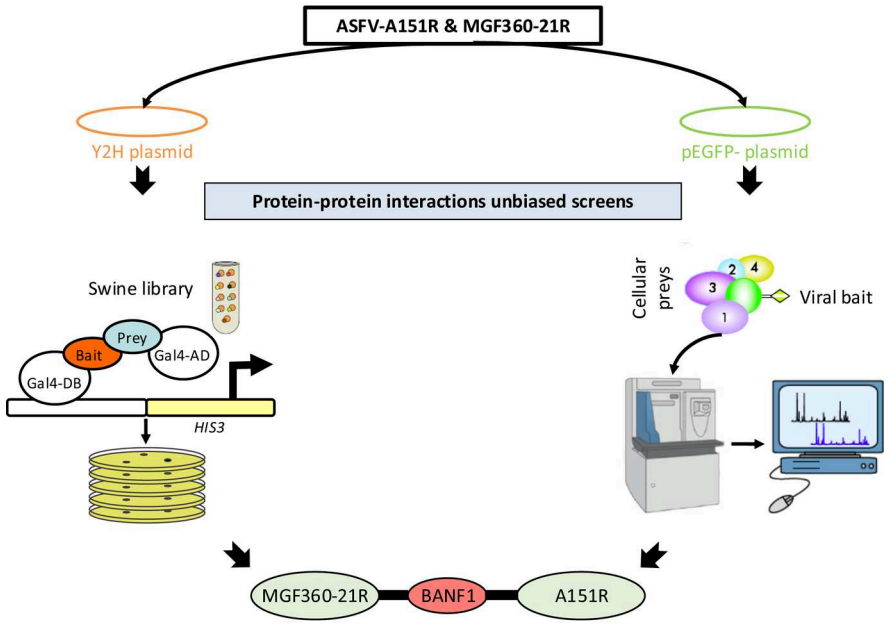

2025, Mol Cell Proteomics *24*(*9*), 101038

https://doi.org/10.1016/j.mcpro.2025.101038

Highlights

- BANF1 was identified as a common interactor of MGF360-21R and A151R ASFV proteins.
- BANF1 silencing reduced ASFV replication, indicating its proviral role.
- Both MGF360-21R and A151R modulate the type I IFN response.
- We have established the interactome of BANF1 in the context of ASFV infection.

Exploring Virus–Host Interactions Through Combined Proteomic Approaches Identifies BANF1 as a New Essential Factor for African Swine Fever Virus

Juliette Dupré[1,2,‡], Katarzyna Magdalena Dolata[3,*,‡], Gang Pei[4], Aidin Molouki[5], Lynnette C. Goatley[5], Richard Küchler[3], Timothy K. Soh[6,7,8,9], Jens B. Bosse[6,7,8,9], Aurore Fablet[1], Mireille Le Dimna[2], Grégory Karadjian[10], Edouard Hirchaud[11], Christopher L. Netherton[5], Linda K. Dixon[5], Ana Luisa Reis[5], Damien Vitour[1], Marie-Frédérique Le Potier[2], Axel Karger[3,*,‡], and Grégory Caignard[1,*,‡]

African swine fever virus (ASFV) causes a lethal disease in pigs and represents a significant threat to the global pork industry due to the lack of effective vaccines or treatments. Despite intensive research, many ASFV proteins remain uncharacterized. This study aimed to elucidate the functions of two ASFV proteins, pMGF360-21R and pA151R, through comprehensive analysis of their interactions with host proteins. Using affinity purification-mass spectrometry and yeast two-hybrid screening approaches, we identified the host protein barrier-to-autointegration factor 1 (BANF1) as a key interactor of both viral proteins. Biochemical and colocalization assays confirmed these interactions and demonstrated that MGF360-21R and A151R expression leads to cytoplasmic relocation of BANF1. Functionally, BANF1 silencing significantly reduced ASFV replication, indicating its proviral role. Given BANF1's established function in regulating the cGAS/STING-dependent type I interferon (IFN-I) response, we postulated that A151R and MGF360-21R could inhibit this pathway. Using different strategies, we showed that both A151R and MGF360-21R did indeed inhibit IFN-I induction. Generation of ASFV deficient of *A151R* or *MGF360-21R* showed that both mutant viruses enhanced the host IFN response in primary porcine macrophages compared to wild-type virus. However, their capacity to inhibit this pathway could occur through mechanisms independent of BANF1. Proteomic analysis of BANF1 interactors during ASFV infection highlighted potentially roles in chromatin remodeling, nuclear transport, and innate immune response pathways. Altogether, our data provide new insights into ASFV-host interactions, identifying BANF1 as an important new host factor required for replication and uncovering novel functions for A151R and MGF360-21R.

African swine fever virus (ASFV) is a large, enveloped virus classified within the *Asfarviridae* family. It is the causative agent of African swine fever (ASF), a disease that exclusively affects suids. Transmission occurs through direct animal-to-animal contact, ingestion of contaminated meat products, fomites, and via soft ticks of the genus *Ornithodoros*. ASFV represents a significant risk to pig health and food security globally due to the absence of available vaccines or treatments and is a disease notifiable to the World Organisation for Animal Health (WOAH). The high lethality in domestic pigs also makes ASFV a significant threat to the global pig industry and imposes a substantial socio-economic burden on many countries. Its double-strand DNA genome, ranging from 170

From the [1]UMR VIROLOGIE, INRAE, École Nationale Vétérinaire d'Alfort, ANSES Laboratoire de Santé Animale, Université Paris-Est, Maisons-Alfort, France; [2]Swine Virology and Immunology Unit, Ploufragan/Plouzané/Niort Laboratory, Agence Nationale de Sécurité Sanitaire de l'Alimentation, de l'Environnement et du Travail (ANSES), Ploufragan, France; [3]Institute of Molecular Virology and Cell Biology, Friedrich-Loeffler-Institut, Federal Research Institute for Animal Health, Greifswald-Insel Riems, Germany; [4]Institute of Immunology, Friedrich-Loeffler-Institut, Federal Research Institute for Animal Health, Greifswald-Insel Riems, Germany; [5]The Pirbright Institute, Woking, Surrey, United Kingdom; [6]Centre for Structural Systems Biology, Hamburg, Germany; [7]Hannover Medical School, Institute of Virology, Hannover, Germany; [8]Cluster of Excellence RESIST (EXC 2155), Hannover Medical School, Hannover, Germany; [9]Leibniz Institute of Virology (LIV), Hamburg, Germany; [10]UMR BIPAR, Ecole Nationale Vétérinaire d'Alfort, INRAE, ANSES, Laboratoire de Santé Animale, Maisons-Alfort, France; [11]Viral Genetic and Biosecurity Unit, Ploufragan-Plouzané-Niort Laboratory, ANSES, Ploufragan, France

[‡]These authors contributed equally to this work.

*For correspondence: Katarzyna Magdalena Dolata, katarzyna.dolata@fli.de; Axel Karger, axel.karger@fli.de; Grégory Caignard, gregory.caignard@vet-alfort.fr.

https://doi.org/10.1016/j.mcpro.2025.101038

to 193 kb in size, contains a relatively conserved, evolutionarily stable "core region" at its center flanked by regions that are dominated by multigene family (MGF) genes. Due to its large genome, the analysis of ASFV-specific proteins with immunologic reagents is limited by the availability of reagents. Infection of mammalian cells with ASFV triggers the expression of over a 100 viral gene products many of which have been confirmed or identified by mass spectrometry in infected cells (1–3) or in purified virus particles (4). In a recent publication, Cackett and colleagues have identified additional ASFV open reading frames (ORF) by analysis of the transcriptome (5) which, in part, have been confirmed as proteins (1), increasing the already large number of ASFV proteins that can extensively interact with the cellular pathways of the host (6). Although ASFV exhibits genomic resemblance with other large DNA viruses, such as poxviruses and herpesviruses, nearly half of ASFV genes lack any known or predictable function. Intriguingly, MGFs and their predicted protein products do not share significant similarities with other known genes or proteins.

Five distinct MGFs (MGF-100, -110, –300, –360, and –505/530) have evolved through gene duplication by homologous recombination (7). ASFV strains lacking or exhibiting only low virulence in pigs are characterized by gene deletions within MGF360 and MGF505 (8, 9). The naturally attenuated OUR T1988/3 strain, isolated from a tick during the epizootic situation in Portugal at the end of the 20th century (10), is distinguished from virulent strains by the absence of eight genes: *MGF360-10L*, *-11L*, *-12L*, *-13L*, *-14L* and *MGF505-1R*, *-2R*, and *-3R* (11, 12). Other studies have shown that MGF genes can determine the host range (13), ASFV virulence (8, 14), and survival of infected macrophages (15). Notably, MGF360 proteins can affect the host antiviral immune response by inhibiting type I IFN (IFN-α/β) production (16–20), and deleting individual genes can result in attenuation of ASFV virulence (17) as well as a reduction of virus replication in ticks (13). However, the functions of most of these genes remain unknown. We are still missing a comprehensive view of the interactome that MGF360 proteins establish with the host proteome, although such information is instrumental to better understand the ASFV replication cycle and pathogenesis at the molecular level.

To further advance in this direction, we utilized a combination of two proteomics methodologies, affinity tag purification-mass spectrometry (AP-MS) and high-throughput yeast two-hybrid (HT-Y2H), to systematically search for cellular interactors of ASFV proteins. This study was initiated by examining interacting partners of the so far uncharacterized ASFV protein MGF360-21R. First, we used an AP-MS approach in cells infected with ASFV to identify both host and viral partners of pMGF360-21R. This led us to characterize a dense virus-host interactions network around pMGF360-21R, including 232 cellular proteins and one single ASFV protein, pA151R. While the role of A151R in virus replication (21) and virulence *in vivo* (22) is evident, the precise molecular mechanisms underlying its functions remain uncertain. Therefore, using the same AP-MS approach with pA151R as a bait, we identified 33 specific interactors of pA151R, but more interestingly, 48 partners shared with pMGF360-21R, among which BANF1 (Barrier-to-autointegration factor 1, also called BAF) emerged as the main interactor.

BANF1 contributes to multiple cellular processes, including post-mitotic assembly (23–27), nuclear membrane repair (28, 29), DNA damage response pathway (30, 31), and the recruitment of transcription factors (30, 32, 33). Its functions seem to be associated with maintaining genome integrity (34). More recently, BANF1 has also been shown to play a role in the modulation of the IFN-α/β pathway by acting on the cGAS (Cyclic GMP-AMP synthase)-STING (Cyclic GMP-AMP/Stimulator of interferon genes) axis. cGAS represents the most extensively studied among the pattern recognition receptors (PRRs) that are involved in sensing ASFV (35–38). Mechanistically, BANF1 competes with cGAS for DNA binding both in the nucleus and the cytoplasm, thereby preventing cGAS activity on cellular self-DNA (39).

In this report, we first confirmed that BANF1 interacts with both pMGF360-21R and pA151R, employing Y2H, biochemical, and colocalization assays. At the functional level, an RNA interference approach was used to demonstrate the proviral effect of BANF1 in ASFV replication. Subsequently, we explored whether A151R and MGF360-21R play a role in the modulation of the IFN-α/β signaling pathway. Using different strategies, we provide unprecedented evidence for the crucial role of A151R and MGF360-21R in counteracting the induction of the IFN-α/β response and suggest that this inhibition does not involve BANF1. Finally, single *A151R* and *MGF360-21R* deletion mutants were constructed and characterized *in vitro*. Both mutant viruses were unable to efficiently control the induction of the IFN-α/β response in primary porcine macrophages compared to their parental strain. Additionally, the GeorgiaΔA151R mutant showed a growth defect in a multi-step replication kinetics assay, indicating an important role of A151R in the virus replication cycle.

EXPERIMENTAL PROCEDURES

Cell Culture

The HEK293 and the wild boar lung-derived (WSL) cells (40) were supplied by the Friedrich-Loeffler-Institut Biobank (catalog numbers CCLV-RIE 0197 and 0379, respectively). Cells were maintained in Iscove's modified Dulbecco's medium (IMDM) mixed with Ham's F-12 nutrient mix (1:1 [vol/vol]) supplemented with 10% fetal bovine serum (FBS). HEK293T and PK15 cells were maintained in DMEM + Glutamax medium (Fisher) containing 10% FBS (Eurobio), 1 mM sodium pyruvate (Fisher), 1% penicillin-streptomycin (Fisher), and 1% non-essential amino acids (Fisher). IBRS2 cells were maintained in MEM medium (Fisher) supplemented with 1.5% lactalbumin hydrolysate (Sigma), 7% FBS (Eurobio), 1% penicillin-streptomycin (Fisher), and 2.5% Hepes (Fisher). Porcine bone marrow (PBMs)

cells were obtained from the leg bones of 4-to 5-week-old, outbred pigs. Following density gradient centrifugation, using Histopaque-1083, the mononuclear cell fraction was recovered, washed, and maintained in Roswell Park Memorial Institute (RPMI) supplemented with 10% FBS, 1% penicillin-streptomycin, and 100 ng/ml porcine colony-stimulating factor CSF1 (Roslin Tech). All cell types were maintained at 37 °C with 5% CO2.

Plasmid DNA Constructs

A151R and *MGF360-21R* of the Georgia 2007/1 strain were cloned by gene synthesis (Twist Bioscience) into pTWIST-ENTR plasmid. Swine-BANF1 and human-BANF1 were amplified from porcine alveolar macrophages (PAM) and A549 cDNA libraries respectively, using specific primers flanked with the Gateway cloning sites 5′-GGGGACAACTTTGTACAAAAAAGTTGGC and 5′-GGGGACAACTTTGTACAAGAAAGTTGG. PCR products were cloned by *in vitro* recombination into pDONR207 (Gateway System; Invitrogen). ORFs were then transferred from pTWIST-ENTR or pDONR207 into different Gateway-compatible destination vectors, according to the manufacturer's recommendations (LR cloning reaction; Invitrogen) and their sequences were verified (Eurofins). GST, Gal4-BD, GFP, mCherry and 3xFLAG tag fusions were achieved using pDEST27 (Invitrogen), pDEST32 (Invitrogen), pDEST-EmGFP-vivid colors, pmCherry-C1 or pCI-neo-3xFLAG vector, respectively.

Transfer plasmids for the generation of ASFV recombinants were synthesized (Genscript, UK) to express the fluorescent markers mNeonGreen or mScarlet-I under the control of the ASFV P30 promoter, for the deletion of *A151R* or *MGF360-21R*, respectively. The markers' sequences were flanked by around 500 bp of the left and right flanking regions of the genes to be deleted (Fig. 9, *A* and *B*).

Antibodies

The primary antibodies used for immunofluorescence were mouse anti-vimentin (MA1-06908; Thermo Fisher), rabbit anti-BANF1 (ab129184, Abcam), and mouse anti-tubulin (B-5-1-2; Sigma-Aldrich). Additionally, a rabbit antiserum specific for ASFV pB646L (P72) and pCP204L (P30) (41) was used at a dilution of 1:20,000 for immunoblotting. The secondary antibodies were Alexa Fluor 647-conjugated goat anti-rabbit IgG (H+L) (A21245, Invitrogen) and goat anti-mouse IgG (H+L) (A32728, Invitrogen). The primary antibodies used for immunoblotting included mouse anti-tubulin (B-5-1-2; Sigma-Aldrich).

Transfection

HEK293 cells were transiently transfected with a GFP-MGF360-21R, a GFP-A151R, or a GFP vector using a K2 multiplier and K2 transfection reagent (Biontex) following the manufacturer's instructions. WSL cells were transiently transfected with GFP-BANF1 or a GFP vector. At 24 h post-transfection, cells were infected with ASFV. For each bait, three independent biological replicates were prepared for affinity purification.

ASFV Infection in WSL Cells

All experiments with ASFV were performed in a biocontainment facility, fulfilling the safety requirements for ASF laboratories and animal facilities (Commission Decision 2003/422/EC, chapter VIII). ASFV (Armenia/07 isolate) was adapted by serial passaging to more efficient replication in WSL cells. Passage 20 stocks were generated as described previously (42) and used in infection experiments. Cell monolayers were inoculated with ASFV stock dilutions at an MOI of 1 PFU/cell, and supernatants collected from mock-infected cells were used as controls. After inoculation, cells were centrifuged for 1 h at 600*g* and 37 °C. Next, cells were washed three times with phosphate-buffered saline (PBS), replenished with medium containing 5% FBS, and incubated at 37 °C with 5% CO_2. Supernatants were harvested at appropriate times, and progeny virus titers were determined as 50% tissue culture infective doses ($TCID_{50}$) per milliliter (43) on WSL cells.

Experimental Design and Statistical Rationale

Affinity purification was performed to identify interaction partners of GFP-tagged viral proteins pA151R, pMGF360-21R, and the host protein BANF1. For each bait, three independent biological replicates were generated from separately transfected HEK293 or WSL cells. GFP-only transfected cells served as negative controls to account for non-specific binding. All samples were processed in parallel under identical conditions to minimize technical variability. Sample size was based on prior studies, balancing statistical power and resource constraints. No technical replicates were performed. Identified proteins were analyzed using Perseus software (v.2.0.10.0) (44) and a protein was considered present if ≥ 2 unique peptides were detected in ≥ 2 out of 3 replicates. Proteins specifically binding to pMGF360-21R, pA151R, or BANF1 baits were filtered out by removing the GFP background. The background list consists of proteins identified in our GFP negative controls and proteins identified as common protein contaminants for AP-MS experiments in HEK293 cells and deposited in the Contaminant Repository for Affinity Purification (CRAPome) (45). Protein abundances were normalized, and enrichment over controls was calculated to identify specific interactors. Statistical significance was determined using two-sample *t* test with Benjamini–Hochberg correction. Potential interactors were considered specific if they were identified only in GFP-bait pulldowns or if the log2 fold change (between GFP control and GFP-bait) was greater than 2 and the *p*-value of a two-sided *t* test was <0.01.

For BANF1 knockdown experiments, WSL cells were transfected with short interfering RNA (siRNA) targeting BANF1 or a non-targeting control, each in triplicate. The student's *t* test was used to evaluate the significance of differences between groups. Statistical analyses were performed using Perseus software and statistical significance was defined as $p < 0.05$.

Affinity Purification and Mass Spectrometry

Affinity Purification—A total of 5×10^6 cells were seeded for each AP experiment. After an overnight incubation, cells were transiently transfected for 24 h before infection with ASFV. At 24 h post-infection and 48 h post-transfection, cells were washed, lysed, and affinity purified on 50 µl GFP-trap agarose beads (Chromotek) as described previously (46).

On-Bead Digestion—Bead-bound proteins were suspended in 300 µl freshly made UA buffer (8 M urea, 100 mM Tris-HCl, pH 8.0), loaded onto 10-kDa filter units (Sartorius), and centrifuged at 12,000*g* at 20 °C for 30 min. Filter-aided sample preparation (FASP) trypsin digestion was performed as described previously (47). Proteins were trypsinized on beads in 100 µl of digestion buffer (1 M urea, 50 mM Tris-HCl, pH 7.5, and 5 µg/ml trypsin (V5111, Promega)). Digestion was performed overnight at 37 °C with shaking. The next day, the peptide-containing supernatant was collected by ultrafiltration and acidified with formic acid (FA, 1% final concentration). Peptides were desalted using C18 100-µl tips (Thermo Scientific) according to the manufacturer's instructions, dried by vacuum centrifugation, and reconstituted in 20 µl of 0.1% FA before mass spectrometry.

MS Data Acquisition and Analysis—Samples were analyzed on a timsTOF Pro mass spectrometer coupled to a nanoElute nanoflow liquid chromatography system (Bruker Daltonics). Peptides were separated on a reversed-phase analytical column (10 cm × 75 µm i.d., Bruker #1866154) by application of a binary gradient made from 0.1% FA in water (solvent A) and 0.1% FA in acetonitrile (solvent B).

During chromatography, solvent B was raised over 60 min (2%–4% from 0 to 1 min, 4%–20% from 1 to 46 min, and 20%–32% from 46 to 60 min) at a constant flow rate of 250 nl/min. The column temperature was maintained at 40 °C. MS analysis of eluting peptides was performed in dda-PASEF mode (1.1-s cycle time) as recommended by the manufacturer. Proteomic data were searched against an ENSEMBL *Homo sapiens* proteome (19,558 entries, v.GRCh38.p13) or a *Sus scrofa* proteome (22,041 entries, v.11.1.2021–11–10) (48) and an NCBI ASFV Georgia (195 entries, v.FR682468.2) (49) proteome database using MaxQuant (v.2.0.3.0) (50) with the following default settings (1): digestion mode was set to specific with Trypsin/P and a maximum of two missed cleavages (2); Carbamidomethyl (C) was selected as a fixed modification (3); oxidation (M) and Acetyl (Protein N-term) were included as variable modifications; and (4) mass tolerances were set to 20 ppm for precursor and 0.5 Da for fragment ions. The false discovery rates (FDR) on the peptide and protein levels were set to 1%, the minimum peptide length was seven amino acids, and the match-between-runs option was used with a 0.7-min match window and 20-min alignment time.

Term Enrichment Analysis and Interaction Network

Porcine genes corresponding to the identified proteins were assigned to their human orthologs using the R package gprofiler2 (v.0.2.1) (51). The interactors of each bait were tested for enrichment of gene ontology (GO) biological processes, Kyoto Encyclopedia of Genes and Genomes (KEGG) annotations, and Reactome terms. The overrepresentation analysis was performed using the enricher function of the clusterProfiler (v.4.2.2) (52) package in R with default parameters. GO terms clustering analysis was performed using the R package rrvgo (v.1.6.0) (53). Selected proteins from significantly enriched functional groups were manually curated, and the network diagram was plotted using Cytoscape (v.3.7.2) (54) with the Cytoscape StringApp plugin (55).

Yeast Two-Hybrid (Y2H) Screening Procedure

Our Y2H protocol closely followed the methodology previously described (56). ORFs encoding *A151R* and *MGF360-21R* were fused with a Gal4 DNA-binding domain (Gal4-BD), within the pDEST32 vector (Invitrogen). These constructs were transformed into the Y2H Gold yeast strain (Clontech) and selected on a selective medium lacking leucine (-L). Y2H screens were performed using a swine cDNA library, which was generated with mRNAs extracted from PAM and then cloned into the Gal4 transactivation domain (Gal4-AD) pDEST22 vector (Creative Biogene). For each screen, at least 30 million yeast diploids were produced and grown on selective medium lacking leucine, tryptophan, and histidine (-L, -W, -H) and supplemented with 5 mM of 3-aminotriazole (3-AT). After 6 days, yeast colonies were picked and purified over 3 weeks by culture on selective medium -L, -W, -H + 5 mM of 3-AT to eliminate false-positives (57). Yeast colonies were lysed using zymolyase (Euromedex), and AD-cDNAs were amplified by PCR. Those PCR products were sequenced (Eurofins), and cellular preys were identified by a multiparallel BLAST analysis.

GST Pulldown Experiments

HEK293T cells were plated in a six-well plate at a density of 2×10^6 cells/well and transfected 24 h later (JetPRIME, Polyplus) with 500 ng of pDEST21 encoding GST-BANF1 (swine or human) and 3x-flag-tagged A151R or MGF360-21R expressed in pCI-neo-3xFLAG. After 36 h, cells were harvested in PBS and incubated in ice-cold lysis buffer (20 mM MOPS-KOH, pH 7.4, 120 mM KCl, 0.5% Igepal, 2 mM β-Mercaptoethanol) and supplemented with Complete Protease Inhibitor Cocktail (Roche) for 20 min. The cell lysates were then clarified at 14,000*g* for 30 min. Protein extracts were incubated for 2 h at 4 °C on a spinning wheel with 30 µl of glutathione-sepharose beads (Amersham Biosciences). The beads were washed three times for 5 min with lysis buffer on a spinning wheel, and samples were boiled in denaturing loading buffer (Invitrogen).

Microscale Thermophoresis Analysis

The binding of pA151R and pMGF360-21R to BANF1 was measured by microscale thermophoresis (MST). After purification, the concentration of GFP-A151R was measured with the fluorescence-based method by normalizing the fluorescence intensity of GFP-A151R to the FITC standard curves as described before (58). 20 nM GFP or GFP-A151R proteins in MST buffer (50 mM Tris-HCl, pH 7.5, 150 mM NaCl, 10 mM DTT) were incubated with different concentrations of ligands. Immediately, samples were loaded into standard glass capillaries (NanoTemper) and thermophoresis analysis was performed on a NanoTemper Monolith NT.115 instrument (40% LED, 80% MST power) at 22 °C. A laser on-time of 30 s and a laser off-time of 5 s were used. The experiment was performed in triplicates, and the MST curves were fitted using NT analysis software to obtain the Kd values.

Immunoblotting

Samples were heated for 5 min at 95 °C and resolved by SDS-polyacrylamide gel electrophoresis (SDS-PAGE) on 4 to 20% Mini-Protean TGX gels (Bio-Rad) (59) and transferred to the nitrocellulose membrane by semidry transfer (Trans-Blot Turbo; Bio-Rad Laboratories) (60). All membranes were blocked in 5% milk powder in Tris-buffered saline with 0.25% Tween-20 (TBST) and probed for a minimum of 1 h at room temperature with the indicated primary antibodies using appropriate dilutions. GST and 3xFLAG-tagged proteins were detected with a rabbit polyclonal anti-GST antibody (1:2500, Sigma-Aldrich) and a mouse monoclonal HRP-conjugated anti-FLAG antibody (M2 1:10,000; Sigma-Aldrich), respectively. Next, membranes were incubated with peroxidase-conjugated secondary antibodies diluted in TBST. Protein bands were detected using the Clarity Western enhanced chemiluminescence (ECL) substrate (Bio-Rad), imaged on a C-DiGit blot scanner (LI-COR), and analyzed with Image Studio software (v.5.2).

Colocalization Assays

IBRS2 cells were plated in 24-well plates (Ibidi) with 1×10^5 cells/well. 24 h later, cells were transfected with either 250 ng of N-EmGFP-DEST Vector expressing either A151R or MGF360-21R and 250 ng of pmCherry-C1 encoding swine_BANF1. 24 h post-transfection, cells were fixed using a 4% paraformaldehyde (PFA) solution (Electron Microscopy Sciences) for 30 min and treated with PBS-glycine (0.1 M) for 5 min. DNA was stained with a Hoechst 33,342 dye (1/10,000) (Life technologies) for 30 min. Finally, cells were visualized using a Leica DMI 8 confocal microscope (×40 magnification).

Immunofluorescence Microscopy

Coverslips with cells were fixed with 3.7% formaldehyde in PBS at room temperature for 60 min. Following fixation, cells were permeabilized with 0.01% TritonX-100 in PBS for 15 min and then blocked with PBS containing 10% FBS for 1 h. Coverslips were incubated with the primary antibody for 1 h at room temperature. Following washing with PBS, cells were incubated with a secondary antibody for 1 h at room temperature. Coverslips were then washed in PBS, and DNA was stained for 15 min with 1 µg/ml Hoechst 33,258 (Sigma-Aldrich). Coverslips were mounted on glass slides using ProLong Glass Antifade Mountant (Invitrogen). Single-slice fluorescence images were acquired on a Leica DMI6000 TCS SP5 confocal

laser scanning microscope (63× objective) and were processed with ImageJ software (v.1.52a) (61).

Gene Silencing by siRNA

Pooled siRNA against porcine or human BANF1 was custom-synthesized and purchased from siTOOLs Biotech together with a nonspecific siRNA negative control. Transfections of siRNA were performed with Lipofectamine RNAiMAX (Thermo Fisher Scientific) following the manufacturer's instructions. The proteome changes after BANF1 knockdown were analyzed by LC-MS/MS analysis. Lysates of WSL knockdown BANF1 (si-BANF1) and control nonspecific siRNA (si-NegC) cells (100 μg) were prepared using the Thermo EasyPep Mini MS sample preparation kit (Thermo Scientific) according to the manufacturer's instructions. Dried peptides were reconstituted in 0.1% FA to a final concentration of 100 ng/μl. Peptides corresponding to 200 ng protein were measured by LC-MS/MS and analyzed as described in "MS data acquisition and analysis."

Luciferase Reporter Gene Assays

HEK293T cells were plated in 24-well plates with 5×10^5 cells/well. After 24 h, cells were transfected (jetPRIME, Polyplus) with either 3x-FLAG-tagged A151R or MGF360-21R along with 300 ng of IFN-β-pGL3 or pISRE-Luc plasmid (0.3 mg/well, Stratagene) that contains the firefly luciferase reporter gene downstream of an IFN-β-specific promoter sequence or the ISRE enhancer element, respectively. Cells were also co-transfected with the normalization pRL-CMV plasmid (0.03 mg/well, Promega) as well as plasmids encoding indicated proteins (RIG-I or cGAS/STING) to stimulate the IFN-β-specific promoter. When specified, cells were transfected 24 h later with 0.1 mg/well of poly(dA:dT) (Invivogen) or treated with 1×10^3 IU/ml of recombinant IFN-β (PBL Assay Science). After 48 h post-transfection, cells were lysed (Passive lysis buffer, Promega), and both firefly and Renilla luciferase activities were detected using the Bright-Glo and Renilla-Glo luciferase assay system, respectively (Promega). Luminescence was measured using the GloMax plate reader (Promega). All graphs depict the mean ratios between luciferase and Renilla of triplicate samples, and error bars of the standard deviation were calculated using Prism 7, version 7.0.

Assessment of IFNβ Levels by RT-qPCR

PK15 cells were plated in 24 wells plates with 5 x 10^5 cells/well. 24 h later, cells were transfected (jetPRIME, Polyplus) with either 300 ng of 3x-FLAG-tagged A151R or MGF360-21R and, when indicated, with 1 μg of interferon stimulatory DNA (ISD, Invivogen) or 100 ng poly(dA:dT) (Invivogen). After 36 h, total RNAs were extracted (RNAeasy kit, Qiagen) RT-qPCR assays were performed using the QuantiNova SYBR Green RT-PCR kit (Qiagen) to measure the expression of the swine *IFN-β* gene. The data were then analyzed using the 2ΔΔCt method, where the amount of target, normalized to the endogenous reference *GAPDH* gene and relative to an experimental control. The results are expressed as relative fold change (Fc) in comparison with the non-stimulated condition.

Computational Modeling of Protein Complexes

Protein complex predictions were generated using the ColabFold version 1.5.5 (62) implementation of AlphaFold-Multimer (63). Various complex stoichiometries between MGF360-21: BANF1 (1:1–2:2) and A151R:BANF1 (1:1–5:2) were predicted and the model confidences assessed. A total of 5 models were predicted for each candidate complex with 3 recycling. Model relaxation and energy minimization were performed using the integrated Amber module. The confidence of resulting protein complex predictions was assessed based on the predicted aligned error (PAE) scores using an in-house Python script available at https://github.com/QuantitativeVirology/AlphaFold_Analysis, file score_colabfold_pairwise.py. For each pairwise combination in a multi-polypeptide prediction, the relevant portion of the PAE plot was extracted. It was evaluated by two criteria: 30 (the maximum value) minus the minimum of the PAE portion (to measure the most confident value) and percent standard deviation (to measure how broad the distribution of confidence values is, i.e., if there are both high confidence and low regions).

Purification of Georgia/2007 Recombinant Viruses

Recombinant gene deleted ASFV was produced by homologous recombination followed by single cell sorting. Briefly, WSL cells were infected with Georgia/2007 WT virus and transfected with the transfer plasmids described above. Single cells expressing either mNeonGreen (ΔA151R) or mScarlet-I (ΔMGF360–21R) were isolated via fluorescence-activated cell sorting (FACS) into purified PBMs as previously described (64). After three rounds of single cell sorting and two rounds of limiting dilutions, viral DNA was extracted using MagVet universal isolation kit (Thermo Fisher Scientific), and the KingFisher flex extraction system (Thermo Fisher Scientific). Deletion of target genes and the absence of parental virus was confirmed by PCR using appropriate internal primers. Full-genome sequencing of the recombinants was done was done as previously described using an Illumina MiSeq instrument (65). Raw reads are available at the Sequence Read Archive in BioProject https://www.ncbi.nlm.nih.gov/sra/PRJNA1183819.

Multistep Growth Curve

PBMs were seeded at 4×10^5 cells per well and infected at MOI of 0.01. Both cells and supernatants were collected at the indicated time points and freeze-thawed twice. Debris were pelleted by centrifugation and titrations were performed using PBMs from two different pigs. Virus titrations were carried out in quadruplicate by haemadsorption assay (HAD_{50}/ml) and titers were calculated using the Spearman and Kärber algorithm. Two-way analysis of variance (ANOVA) followed by Dunnett's multiple-comparison test was used to evaluate the differences between titers at different times post infection.

Quantification of IFN-α and CXCL10 Levels in Supernatants

Purified PBMs from an outbred pig were seeded at 1 x 10^6 cells/ml and infected with recombinant or wild-type viruses at a MOI of 0.5. After 1 h incubation the inoculum was removed and replaced with fresh medium. The supernatants were collected at 8 and 16 h post infection and centrifuged at 300*g* for 5 min to remove cells and debris. The levels of IFN-α in these supernatants were then evaluated using an in-house ELISA. Briefly, Maxisorp plates (Nunc) were coated with anti-pig IFN-α antibody (clone K9) at 0.5 μg/ml in 0.05 M coating buffer overnight at room temperature. Plates were washed with PBS-T (0.05% Tween 20 in PBS) and blocked with 1% bovine serum albumin (BSA) in PBS. Standards (recombinant porcine IFN-α, PBL Assay Science) and samples were then added in duplicate and incubated at room temperature for 2 h. Following washing, biotinylated anti-pig IFN-α antibody (clone F17) diluted 1:5000 in blocking buffer was added to the wells and incubated for 2 h at room temperature. The plates were then washed, incubated with streptavidin-horseradish peroxidase (R&D Systems, DY998), and finally developed with 3,3′,5,5′-tetramethylbenzidine (TMB) substrate (R&D Systems, DY999). After stopping the reaction with 2 N H_2SO_4, the absorbances were read at 450 nm. The concentration of CXCL10 in the supernatants was quantified using the swine CXCL10 Do-It-Yourself ELISA (Kingfisher Biotech). Briefly, Maxisorp plates were coated overnight with capture antibody (anti-swine CXCL10

polyclonal antibody, PB0119S-100) at 2.5 μg/ml in PBS. The plates were then washed with PBS-T and blocked with 4% BSA for 1 h at room temperature. Samples and standards were then added, and the plates were incubated at room temperature for 1 h. After four washes with PBS-T, detection antibody (biotinylated anti-swine CXCL10 polyclonal antibody, PBB1138S-050), diluted in blocking buffer at 0.05 μg/ml, was added to plates, and incubated for another hour at room temperature. The plates were then washed, incubated with streptavidin-horseradish peroxidase and developed as described earlier. Two-way analysis ANOVA followed by Dunnett's multiple-comparison test was used to evaluate the differences between IFNα and CXCL-10 concentrations in the supernatants at different times post infection.

RESULTS

Identification of Host and Viral Proteins Interacting With ASFV MGF360-21R and A151R by AP-MS

To gain functional information about the previously uncharacterized ASFV protein pMGF360-21R, we analyzed its interactions with the host and viral proteins in infected cells. To begin with, pMGF360-21R of the highly virulent ASFV strain Georgia 2007/1 (66) fused to an N-terminal green fluorescent protein (GFP) tag was expressed in HEK293 cells and subsequently AP-MS was performed to identify its interactors (Fig. 1*A*). GFP alone was employed as a negative control. Interacting proteins were purified with a GFP-trap system and subjected to MS analysis in biological triplicates. We compiled a list of background proteins to filter out nonspecific binders from true protein interactors (Supplemental Table S1*A*). In this way, we selected 232 protein interactions for pMGF360-21R (Supplemental Table S1*B*). The top five ranked high-confidence proteins, based on their abundance, sequence coverage, and probability score, were ASFV protein pA151R, elongins B and C (ELOB and ELOC), and two pyrroline-5-carboxylate reductases (PYCR1 and PYCR2) (Fig. 1*B*). Notably, A151R emerged as both a high-confidence interactor and the only viral protein interacting with pMGF360-21R. Therefore, we also analyzed the interactome of N-terminally GFP-tagged pA151R in infected HEK293 cells by AP-MS (Supplemental Table S1*C*). This allowed us to compare the interactomes of

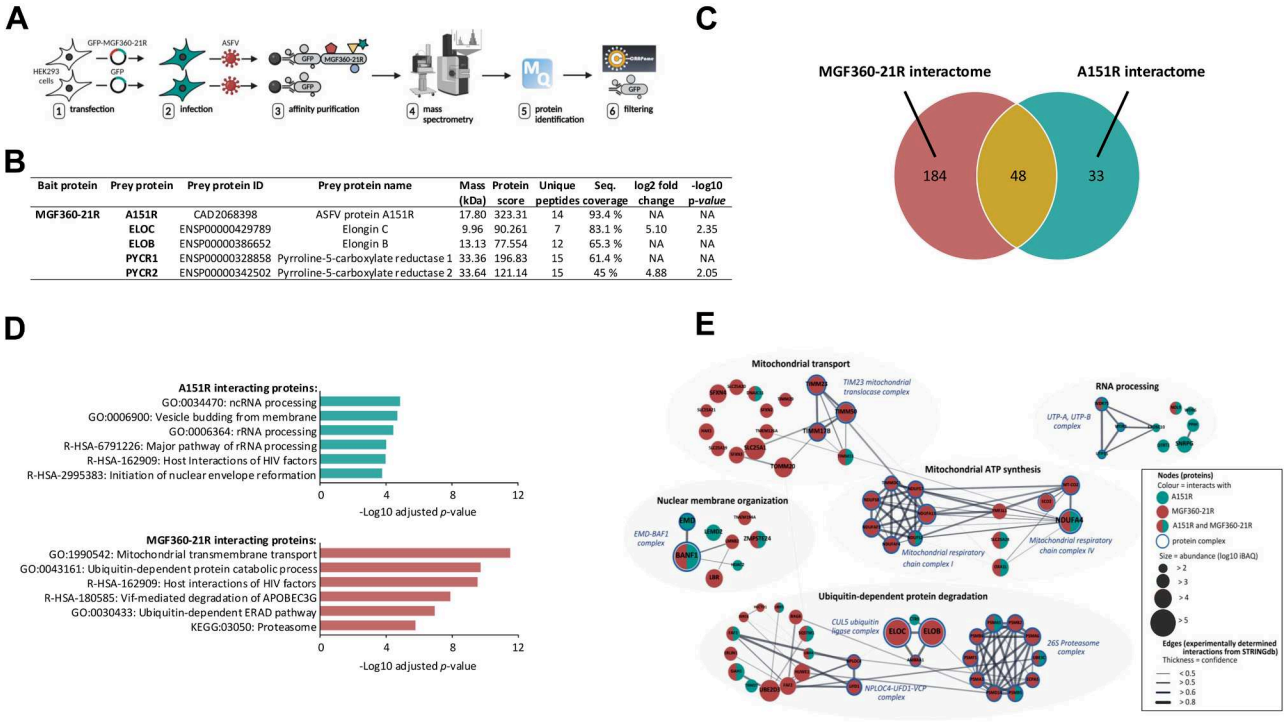

Bait protein	Prey protein	Prey protein ID	Prey protein name	Mass (kDa)	Protein score	Unique peptides	Seq. coverage	log2 fold change	-log10 p-value
MGF360-21R	A151R	CAD2068398	ASFV protein A151R	17.80	323.31	14	93.4 %	NA	NA
	ELOC	ENSP00000429789	Elongin C	9.96	90.261	7	83.1 %	5.10	2.35
	ELOB	ENSP00000386652	Elongin B	13.13	77.554	12	65.3 %	NA	NA
	PYCR1	ENSP00000328858	Pyrroline-5-carboxylate reductase 1	33.36	196.83	15	61.4 %	NA	NA
	PYCR2	ENSP00000342502	Pyrroline-5-carboxylate reductase 2	33.64	121.14	15	45 %	4.88	2.05

FIG. 1. **Interactome of MGF360-21R and A151R in ASFV-infected HEK293 cells.** *A*, AP-MS experimental workflow for identifying host and viral proteins interacting with MGF360-21R. *B*, Top 5 high-confidence proteins identified as interactors for MGF360-21R in AP-MS experiments. "NA" (Not Available) indicates that the protein was not detected in the GFP control, so fold change and statistical comparison could not be performed. *C*, *Venn diagram* of proteins identified by AP-MS in ASFV-infected HEK293 cells expressing MGF360-21R-GFP or A151R-GFP. *D*, term enrichment profiles of A151R and MGF360-21R interactomes. The most significant GO, KEGG, and Reactome terms are shown with Benjamini-Hochberg corrected *p*-values. *E*, network of host proteins interacting with A151R (*green* nodes), MGF360-21R (*red* nodes), or both proteins (*half green, half red* nodes) clustered by enriched terms in GO, KEGG, or Reactome. Node sizes scale with protein abundances (log10 iBAQ). Protein complex constituents are indicated as nodes with *blue border* and the respective complex names according to the EBI Complex Portal are presented as *blue* descriptions. *Edges* indicate the protein-protein interactions based on the available experimental evidence, and *edge thickness* represents the confidence prediction of the interaction from the STRING database. Detailed information is provided in Supplemental Table S1*E*.

both viral proteins and to distinguish common and specific interaction patterns regulating MGF360-21R and A151R functions during viral infection. We identified 48 common interactors (Fig. 1*C*). Additionally, 184 specific interactions were identified for pMGF360-21R and 33 for pA151R. The GO term enrichment analysis (67) and pathway enrichment analysis using the KEGG database (68), or the Reactome database (69) showed that pA151R interactors were significantly enriched in RNA processing and nuclear envelope reformation proteins (Fig. 1*D*, Supplemental Table S1*D*). The proteins interacting with pMGF360-21R were enriched for terms related to mitochondrial transport (GO:1990542) and ubiquitin-dependent protein degradation (GO:0043161). Next, we focused on proteins from enriched terms and assembled a host-virus interaction network of proteins binding pA151R and/or pMGF360-21R (Fig. 1*E*). We used the STRING database (70) to identify interactions between host proteins that have been experimentally validated and the EBI Complex Portal (71) database to assign the proteins into specific protein complexes (Supplemental Table S1*E*).

Mapping Cellular Interactors of ASFV MGF360-21R and A151R by Y2H

Complementary to the AP-MS approach, a porcine cDNA library was screened by HT-Y2H using pMGF360-21R and pA151R viral proteins from Georgia 2007/1 as baits. The schematic representation of the HT-Y2H screening protocol is illustrated in Figure 2*A*. Each screen was performed by yeast mating to obtain a minimum of 30×10^6 diploids, a number corresponding to 10 times the complexity of our cDNA library. A total of 311 positive [His+] yeast colonies were recovered from these two screens (132 and 179 clones for MGF360–21R and A151R, respectively), and cellular prey proteins were identified by cDNA amplification, sequencing, and multi-parallel BLAST analysis. Four interactors were identified for MGF360-21R, with cytochrome c oxidase subunit 2 (COX2) and small ribosomal subunit protein uS19 (RPS15) appearing once each while TCF3 fusion partner (TFPT) was found 16 times (Fig. 2*B*). Interestingly, BANF1 emerged as a common interactor of pMGF360-21R (114 times) and pA151R (179 times), also being the only interactor of pA151R. To confirm this result, the full-length porcine BANF1 was retested against MGF360-21R and A151R by Y2H (Fig. 2*C*). As expected, both pMGF360-21R and pA151R were able to interact with BANF1. Among the shared interacting proteins of pMGF360-21R and pA151R, BANF1 represented the highest confidence in both AP-MS and Y2H approaches. Details of the MS analysis confirming the specific binding of BANF1 to both viral proteins are given in Supplementary Figure S1. In addition, the data obtained from Y2H also indicated that BANF1 constitutes a direct binding partner of both, pMGF360-21R and pA151R. Therefore, we comprehensively characterized the interaction between the viral proteins pMGF360-21R and pA151R, along with the host protein BANF1, and explored its significance in the context of ASFV infection.

MGF360-21R and A151R Interact With Both Human and Swine BANF1

To validate the interactions at the biochemical level, 3xFLAG-tagged full-length swine BANF1 was co-expressed in HEK293T together with GST-tagged MGF360-21R or A151R and subsequently complexes binding to the GST-tagged ASFV proteins were affinity purified with glutathione-sepharose beads. As expected, BANF1 co-purified with both pMGF360-21R and pA151R (Fig. 3, *A* and *B*). Moreover, after exchanging swine BANF1 with the human BANF1 in these experiments, binding of human BANF1 to pA151R and pMGF360-21R could also be observed (Fig. 3, *C* and *D*). This validation was crucial, particularly as some of our functional studies were performed with human cells. To determine whether BANF1 directly binds to pMGF360-21R or pA151R and evaluate their corresponding binding affinities, 3xFLAG-tagged swine BANF1, GFP-MGF360-21R, or GFP-A151R were expressed in HEK293T cells and purified using anti-FLAG or GFP affinity agarose. Subsequently, MST was performed to quantify the dissociation constant (K_d). In accordance with the previous co-immunoprecipitation data, direct binding of BANF1 to GFP-A151R was confirmed and a K_d value of 105 ± 31 nM was determined for the complex (Fig. 3*E*). In contrast, a direct interaction between BANF1 and pMGF360-21R could not be observed, indicating that other factors may be involved in the interaction between BANF1 and pMGF360-21R in these conditions. In addition, formation of massive pMGF360-21R oligomers was observed during the purification process, which might have interfered with the formation of a BANF1–pMGF360-21R complex under the conditions of MST measurement. However, structural modeling of complexes between BANF1 and pMGF360-21R with varying stoichiometries using AlphaFold-Multimer resulted in a high-confidence model consisting of one pMGF360-21R molecule and one BANF1 dimer (72) (Fig. 3*F*) therefore we do not exclude the possibility of the formation of a pMGF360-21R–BANF1 complex.

A151R and MGF360-21R Colocalize with BANF1 Both in Porcine and Human Cells

To assess the potential impact of the A151R-BANF1 and MGF360-21R-BANF1 interactions on their respective subcellular localizations, we first carried out fluorescence microscopy using a porcine kidney epithelial cell line, IBRS2. A fusion protein of swine BANF1 with the red fluorescent protein mCherry was co-expressed with GFP-tagged A151R (GFP-A151R) or MGF360-21R (GFP-MGF360–21R) (Fig. 4*A*). When expressed alone, BANF1, pMGF360-21R, and pA151R were localized in the cytoplasm, with pA151R also exhibiting perinuclear localization. Upon co-transfection, mCherry-tagged BANF1 colocalized with both GFP-tagged MGF360-21R

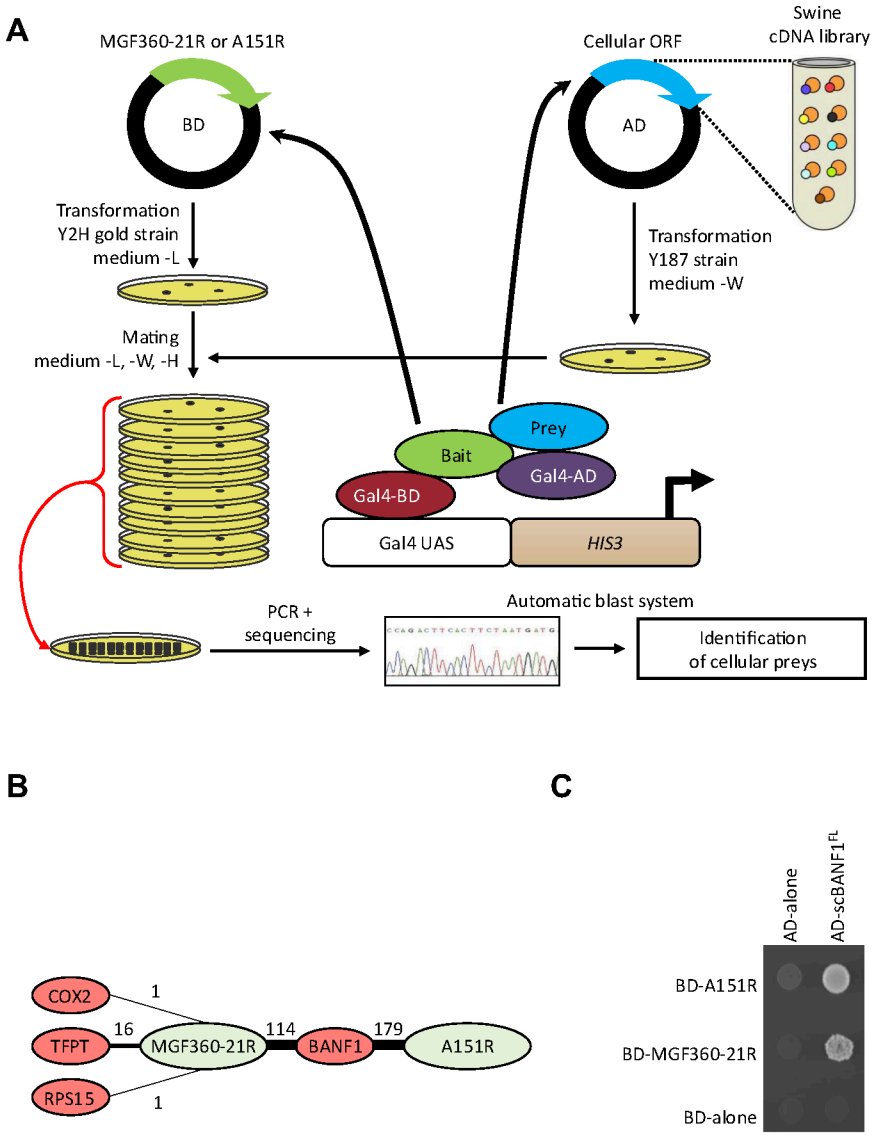

FIG. 2. **Overview of the HT-Y2H Pipeline and data.** *A*, A151R or MGF360-21R (viral bait) is expressed in yeast and tested for host protein interactors by mating with yeast containing libraries of swine cDNA (cellular prey). An interaction between the viral protein and the cellular protein induces transcription of a reporter gene allowing growth on selective media. Then, cDNAs from each colony are amplified by PCR, sequenced and identified by an automatic blast system. *B*, for each interaction, the thickness of the edge corresponds to the number of positive yeast colonies. *C*, interactions of BANF1 with A151R and MGF360-21R were analyzed in the Y2H system. Yeast cells expressing A151R or MGF360-21R fused to the Gal4 DNA-binding domain (BD) were co-transformed with a plasmid encoding the Gal4 transactivation domain (AD) fused to BANF1. Yeast cells were plated on a growth medium supplemented with 5 mM 3-AT to test interactions.

and A151R in the cytoplasm and the perinuclear region. We next examined the subcellular localization of endogenous BANF1 in HEK293 cells in response to the ectopic expression of GFP-A151R, GFP-MGF360-21R, or the GFP tag alone (Fig. 4*B*). In contrast to mCherry-tagged BANF1, endogenous BANF1 was exclusively located within the nucleus when the GFP tag alone was expressed as a control. Interestingly, the expression of either A151R or MGF360-21R induced the translocation of BANF1 to the cytoplasm. Yet these two viral proteins exhibited distinct colocalization patterns with endogenous BANF1: pA151R and BANF1 appeared to concentrate around the cell nucleus, while pMGF360-21R and BANF1 were dispersed in the cytoplasm. Altogether, these results demonstrate that pA151R and pMGF360-21R colocalize with BANF1 in both porcine and human cells.

Relocation of BANF1 during ASFV Infection

As infection with vaccinia virus (VV) and Herpes Simplex Virus 1 (HSV-1) leads to marked changes in the cellular distribution of BANF1 (73, 74), we have studied the relocation of

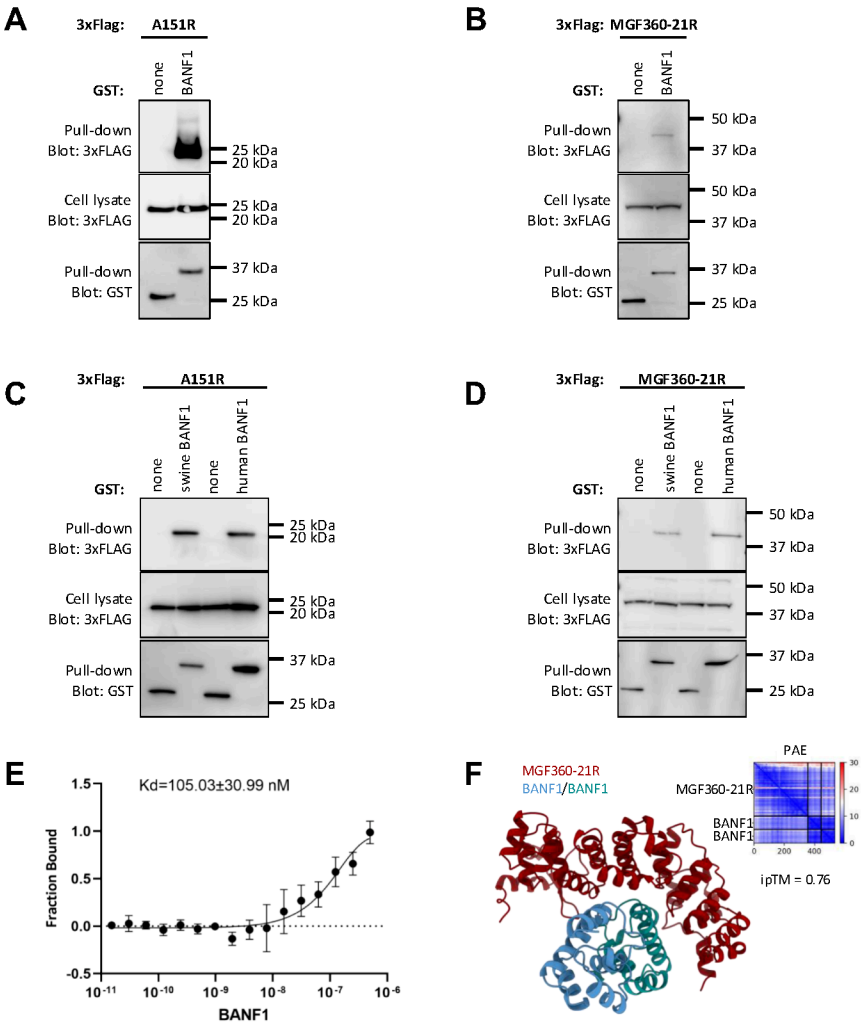

FIG. 3. **Biochemical validation of BANF1 interaction with A151R and MGF360-21R.** *A–D*, HEK-293T cells were transfected with expression vectors encoding GST alone or fused to either A151R (*A, C*) or MGF360-21R (*B, D*) and tested for the interaction with either human (*C, D*) or swine BANF1 (*A–D*). Total cell lysates were prepared 48 h post-transfection (cell lysate, middle panels), and co-purifications of indicated cellular proteins were assayed by pulldown using glutathione-sepharose beads (pulldown, *upper panels*). GST-tagged viral proteins were detected by immunoblotting using anti-GST antibody (pulldown, *lower panels*), while BANF1 was detected with an anti-3xFLAG antibody. Masses are shown in kilodaltons (kDa). *E*, microscale thermophoresis (MST) analysis of direct binding of A151R to BANF1. *F*, predicted structure of the MGF360-21R (*red*) and dimeric BANF1 (*blue* and *green*) complex with an ipTM of 0.76 as ribbon representation. Low PAE values, which indicate high confidence, between protein chains indicate potential interactions.

BANF1 in the context of ASFV infection. Subsequently, we analyzed the subcellular localization of BANF1 in WSL during ASFV infection (Fig. 5*A*). As expected in mock-infected cells, BANF1 was exclusively located in the nucleus. However, we failed to detect BANF1 in the cell at 8 h (h) post infection (p.i.) or observed only minimal protein levels in the cytoplasm at 24 h p.i., suggesting ASFV infection induced BANF1 degradation or obscured its detection by antibodies. To address this question, we reanalyzed the proteomic dataset documenting changes in host protein levels during ASFV infection in porcine WSL cells generated in a prior study (46). We observed no significant changes in BANF1 protein abundance throughout the course of the infection (Fig. 5, *B* and *C*), indicating that BANF1 is not undergoing ASFV-induced degradation.

BANF1 Silencing Reduces ASFV Replication

Given that BANF1 has been demonstrated to function as a retroviral cofactor (75, 76) while also displaying antiviral properties against VV (77) and HSV-1 (74), we decided to examine its influence on ASFV replication in the porcine WSL cell line. For this purpose, BANF1 expression was knocked down by siRNA pools (si-BANF1). In parallel, we used a si-NegC pool as a control. Titration of si-BANF1 ranging from 1 nM to 10 nM revealed effective silencing of BANF1 in WSL cells at concentrations of 3 nM and 6 nM, as confirmed

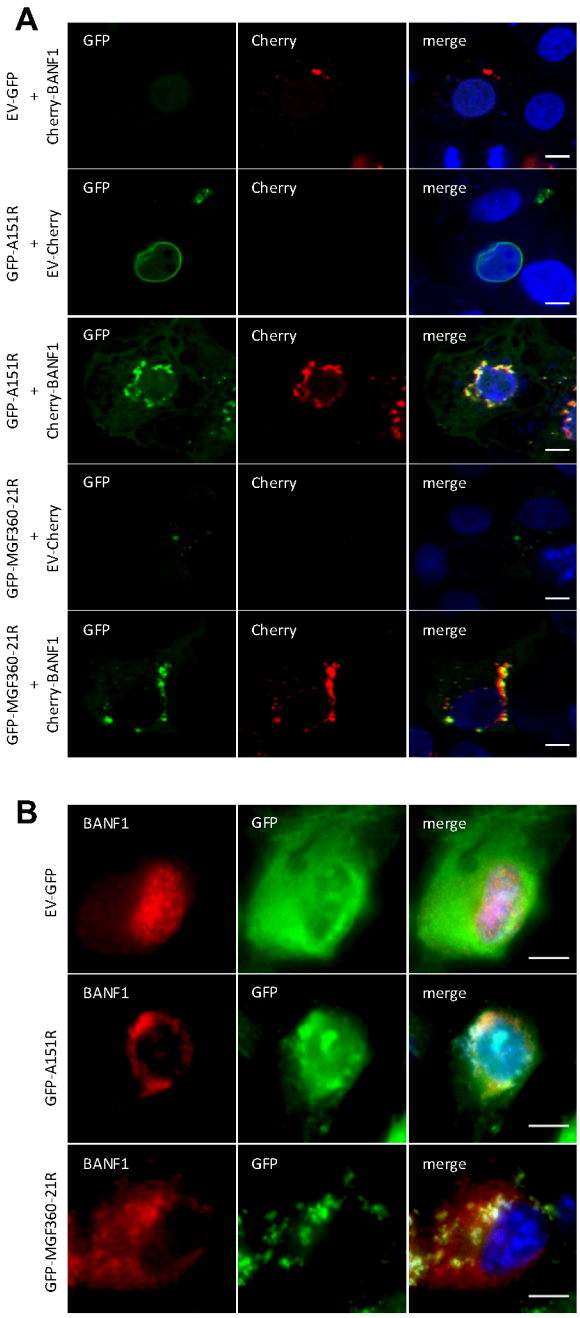

FIG. 4. **Analysis of BANF1 interactions by colocalization assays.** *A*, IBRS2 cells were co-transfected with pEGFP-C1 and pmCherry-C1 plasmids encoding A151R or MGF360-21R and swine BANF1, respectively. After 24 h, cells were fixed and labelled with the dye Hoechst 33,258 to stain nuclei. Intracellular localization of Hoechst-stained nuclei (*blue*), A151R or MGF360-21R (*green*), and BANF1 (*red*) were visualized by confocal fluorescence microscopy (×40 magnification). *B*, same experiment as (*A*) but with HEK293 cells transiently expressing GFP-A151R and GFP-MGF360-21R to test colocalization with endogenous BANF1. Cells were visualized by confocal laser scanning microscope (×63 magnification). *Scale bars* represent 10 μM.

through Western blotting analyses (Fig. 6*A*) and immunofluorescence microscopy (Fig. 6*B*). Importantly, the suppression of BANF1 expression in WSL cells did not decrease cell viability when compared to si-NegC (Fig. 6*C*). Next, WSL cells were transfected with either 3 nM or 6 nM si-BANF1 for 24 h, inoculated with ASFV at a multiplicity of infection (MOI) of 1, and the infection was allowed to proceed for 0, 24, or 48 h. The progeny virus production was reduced by approximately 2-$\log_{10}$ after 24 and 48 h p.i. when using a 6 nM concentration of si-BANF1, in contrast to control cells treated with si-NegC and non-transfected (NT) cells (Fig. 6*D*). We therefore conclude that BANF1 is required for the unimpaired replication of ASFV in WSL cells. To detect any secondary effect of BANF1 downregulation on the inhibition of ASFV production induced, for instance, by impacting the host cell proteome, we performed a comparative proteomic analysis of WSL cells after treatment with si-BANF1 and si-NegC control, respectively. Of the 203 differentially expressed proteins, 92 were exclusively identified in si-BANF1 knockdown cells, and 37 exclusively in si-NegC cells (Fig. 6*E*, Supplemental Table S2). Additionally, 67 proteins were significantly upregulated, and seven significantly downregulated in si-BANF1 treated cells. The suppression of BANF1 led to increased expression of proteins involved in the virus-mediated innate immune response through cGAS-STING, interferon, and RIG-I-like receptor pathways (Fig. 6*F*). BANF1 knockdown also affected the expression of proteins participating in DNA and histone methylation, DNA replication, and nuclear transport. Moreover, the Ser/Thr kinase VRK1 (vaccinia-related kinase 1), responsible for the phosphorylation of BANF1 (77), was only identified in siBANF1 knockdown cells. We also detected changes in the levels of emerin complex proteins (MYOE1, MYH9, ACTB) and zinc metalloproteinase Ste24 homolog (ZMPSTE24), directly implicated in the functioning of BANF1 binding partners, emerin, and lamin A/C (78, 79).

A151R and MGF360-21R Inhibit the Induction of the IFN-α/β Signaling Pathway

Based on our findings presented in Figure 6*F*, and considering the established role of BANF1 in the regulation of the cGAS/STING-dependent IFN response, we hypothesized that A151R and MGF360-21R expression might inhibit this pathway. To answer this question, an IFN-β reporter assay was used. HEK293T cells were co-transfected with a plasmid encoding the luciferase gene under the control of the IFN-β promoter. This could be activated by the plasmid-driven expression of cGAS and STING. The impact of A151R or MGF360-21R on IFN-β expression was measured by co-expression of the viral proteins together with the IFN-β promoter luciferase reporter system and the cGAS/STING inducers. A151R and MGF360-21R efficiently reduced the

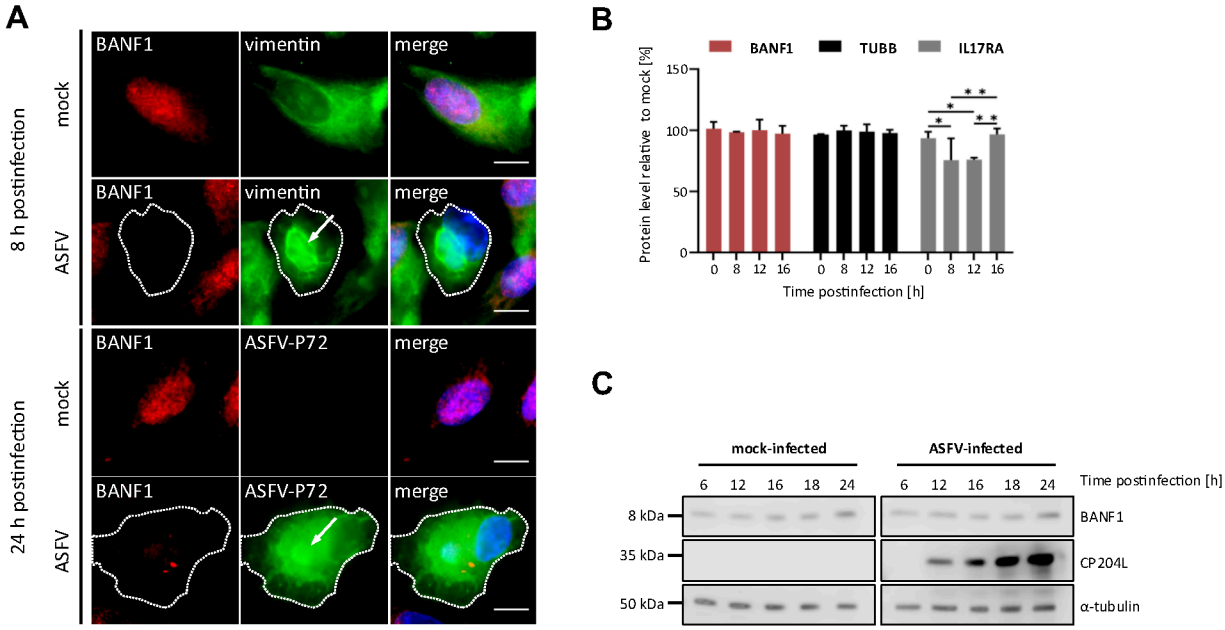

FIG. 5. **Alterations in subcellular localization and abundance of BANF1 during ASFV infection.** *A*, Indirect immunofluorescence shows BANF1 distribution in mock and ASFV-infected WSL cells monitored at 8 and 24 h p.i. Virus replication sites (virus factories), marked with *arrows*, were labeled with antibodies directed against vimentin (at 8 h p.i.) and against ASFV-P72 protein (at 24 h p.i.). *Dotted lines* indicate the outlines of infected cells, *bars* represent 10 μm. *B*, comparison of BANF1 protein levels in mock and ASFV-infected WSL cells based on log10 LFQ (label-free quantitation) values. Levels of tubulin beta chain (TUBB) and interleukin-17 receptor A (IL17RA) are presented as controls. Means of results from three independent replicates and standard deviations are plotted. *, $p < 0.05$; **, $p < 0.01$. *C*, temporal expression of BANF1 in WSL cells, either mock-infected or infected with ASFV. Antibodies against the ASFV protein CP204L and host α-tubulin were used as infection and loading controls, respectively.

stimulating effect of cGAS/STING (Fig. 7*A*). To further assess whether the observed inhibitions were specific to the cGAS/STING axis, we performed the same experiments using cells stimulated with poly(dA:dT), which mimics viral double-stranded DNA, or overexpressed with a constitutively active mutant of RIG-I (NΔRIG-I, N-terminal CARDs of RIG-I). As shown in Figure 7, *B* and *C*, similar inhibitions of IFN-β promoter activity were observed for both pA151R and pMGF360-21R. However, neither of the two ASFV proteins antagonized an IFN-stimulated response element (ISRE)-luciferase gene reporter (Fig. 7*D*) in IFN-β-stimulated cells, indicating that they do not inhibit Jak/STAT signaling and that the antagonism is specific to the IFN induction pathway. Although HEK293T cells are highly efficient for transfection, we aimed to complement our analysis by carrying out equivalent experiments using porcine cells. To do so, we measured the expression level of *IFN-β* mRNAs in porcine PK15 cells treated by either the cytosolic DNA sensor ligands: interferon stimulated DNA (ISD) or poly(dA:dT). As shown in Figure 7, *E* and *F*, we confirmed that A151R and MGF360-21R could also modulate the induction of the IFN-α/β signaling pathway in a porcine *in vitro* model. It should be noted that A151R showed a very strong inhibition of this cellular pathway following ISD stimulation (Fig. 7*E*). To investigate whether the inhibition of IFN-α/β activation by A151R and MGF360-21R was dependent on their interaction with BANF1, we used a gene silencing approach. HEK293T cells were transfected with BANF1-specific or control nonspecific siRNA before transfection with 3xFLAG-tagged A151R or MGF360-21R and stimulation by cGAS/STING or poly(dA:dT) (Fig. 7, *G* and *H*, respectively). In both cases, the reduction of BANF1 expression did not affect the capacity of A151R and MGF360-21R to control IFN-β induction. Under these conditions, we conclude that binding to BANF1 may not represent a molecular mechanism underlying the inhibition of the IFN-α/β pathway by A151R and MGF360-21R.

BANF1 Interactome in ASFV-Infected Cells

Beyond a role in innate immunity, BANF1 facilitates various essential cellular processes by engaging with DNA, histones, and many other nuclear and cytoplasmic proteins (reviewed in reference (34)). To investigate the BANF1 interactome in the context of ASFV infection and DNA binding, we expressed the BANF1-GFP fusion protein in WSL cells under the four following experimental conditions: (i) absence of infection and benzonase treatment (mock-infected, no treatment), (ii) absence of infection and presence of benzonase treatment (mock-infected, benzonase treatment), (iii) presence of ASFV infection and absence of benzonase treatment (ASFV-infected, no treatment), and (iv) presence of ASFV infection and

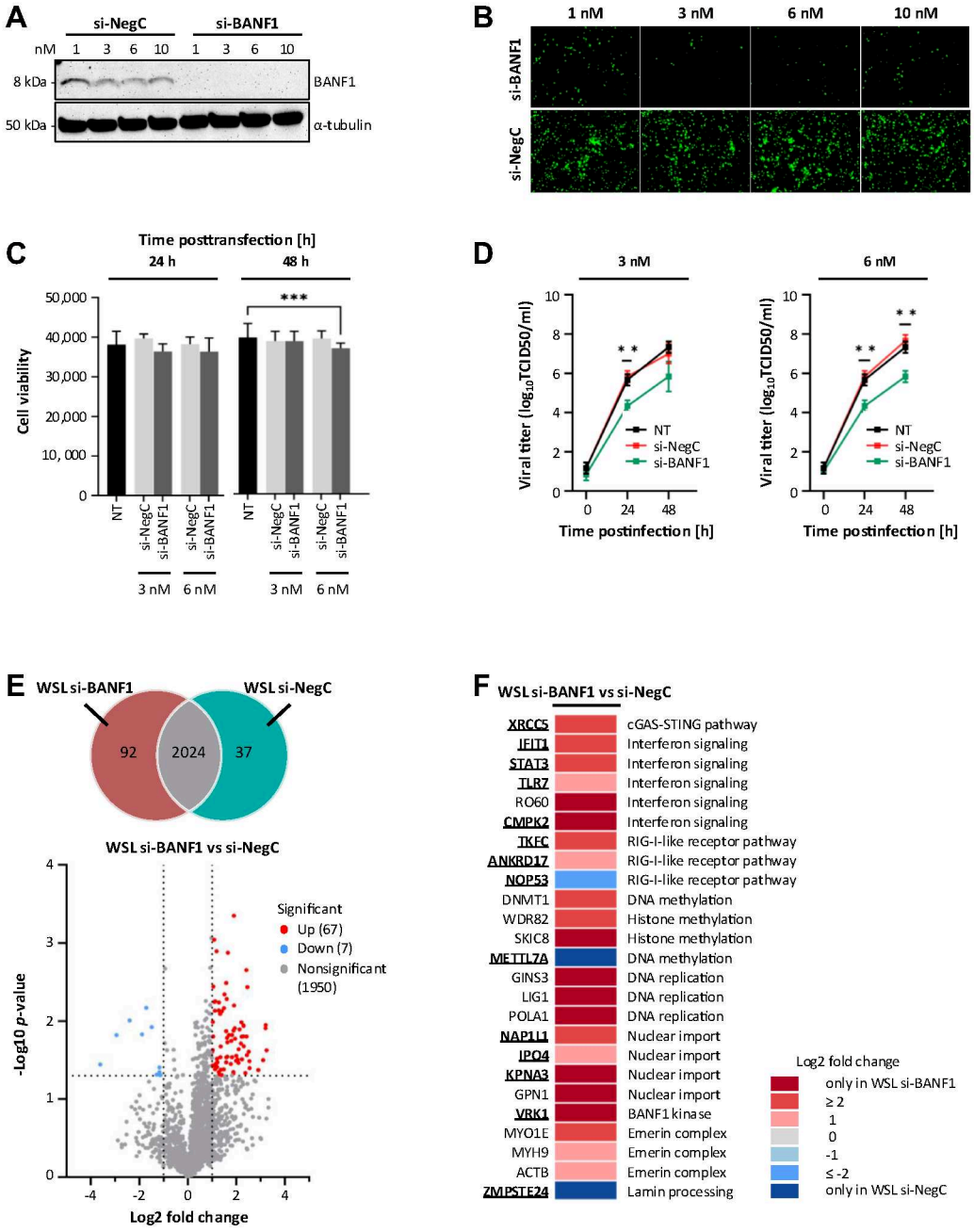

FIG. 6. **The effect of BANF1 downregulation on ASFV replication and the cellular proteome.** *A*, expression of BANF1 in WSL cells transfected with increasing concentrations of si-BANF1 or si-NegC detected by Western blot analyses. The α-tubulin-specific signal was used as a loading control. *B*, immunofluorescence images show endogenous BANF1 in WSL cells transfected with increasing concentrations of si-BANF1 and si-NegC. *C*, cell viability of WSL cells without treatment (NT) or after treatment with si-NegC, or si-BANF1 at the given concentrations was quantitated with a resazurin-based assay (PrestoBlue). Corrected *p*-values below 0.001 are indicated by ***. *D*, growth kinetics of ASFV on WSL cells without treatment (NT) or after incubation with si-NegC and si-BANF1 after infection at a MOI of 1 (n = 3 wells/cell line/time point). The culture medium was collected at the indicated times, and the yields of the cell-free virus were expressed as TCID50 per milliliter and were plotted as means of results from three independent replicates and standard deviations, ** indicates $p < 0.01$. *E*, *Venn diagram* of proteins identified by MS in WSL si-NegC and si-BANF1 knockdown cells (*upper panel*). Volcano plot showing differentially abundant proteins in WSL si-NegC and si-BANF1 knockdown cells (*bottom panel*). The –log10 *p*-value (Benjamini–Hochberg corrected) is plotted against the log2 (fold change: si-BANF1/si-NegC). The *dotted vertical lines* denote ±1.0-fold change on the log2 scale while the dotted *horizontal line* denotes the significance threshold of $p = 0.05$. *F*, Heatmap showing a selection of proteins characterized by significant changes in abundance in WSL cells after si-NegC and si-BANF1 knockdown. Proteins known to be involved in virus replication (see references in Supplemental Table S2) have been highlighted in *bold* and are *underlined*.

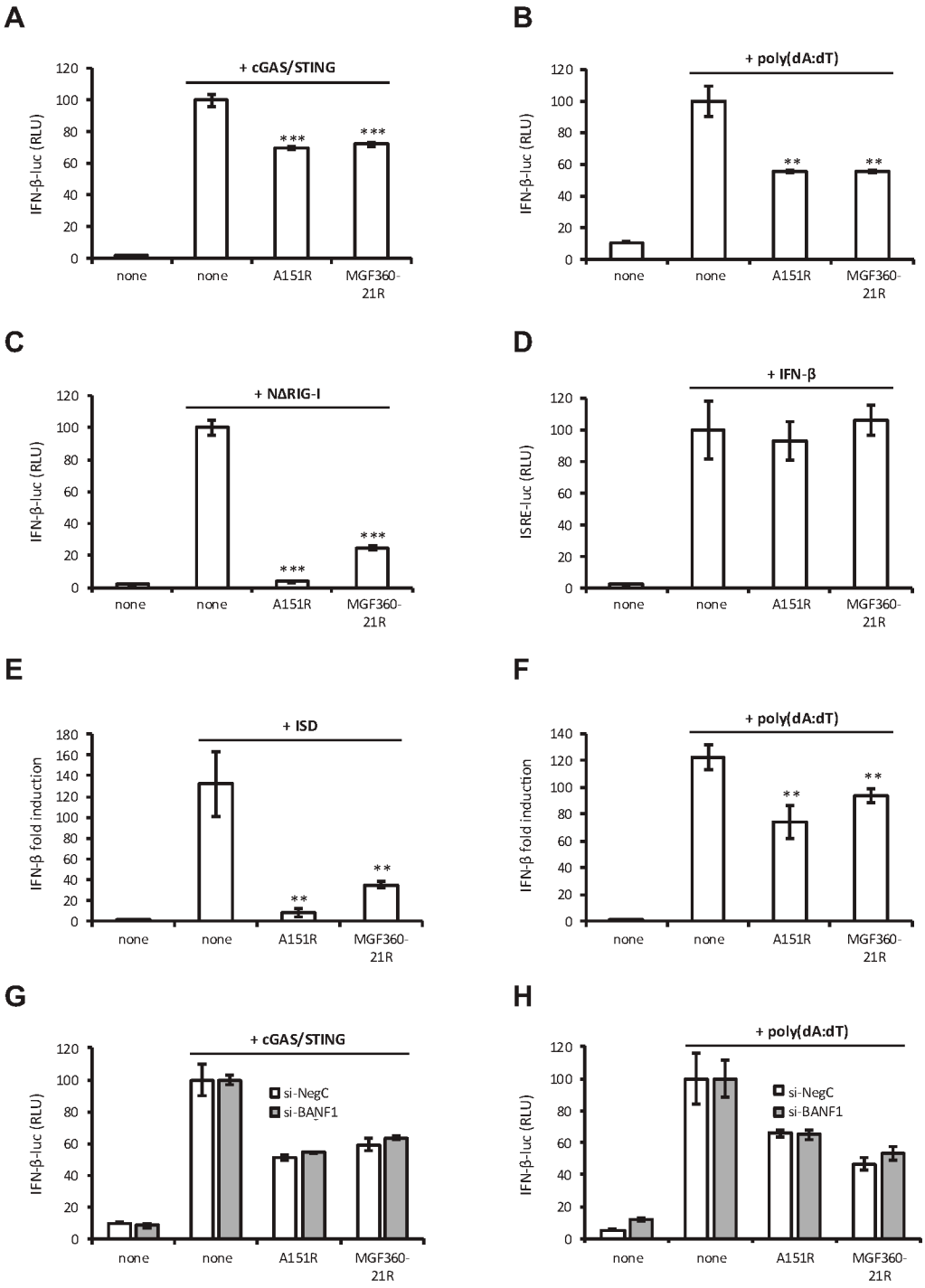

FIG. 7. **Activation of the IFN-β and ISRE promoters in cells expressing A151R and MGF360-21R proteins.** *A*, HEK293T cells were co-transfected with IFN-β-pGL3 and pRL-CMV reference plasmids, pUNO1 plasmids expressing cGAS and STING and pCI-neo-3xFLAG expression vectors encoding 3xFLAG alone or fused to A151R or MGF360-21R. After 48 h, the relative luciferase activity was determined. *B, C*, same experiment as (*A*) but with HEK293T cells transfected with poly(dA:dT) (*B*) or with a plasmid encoding NΔRIG-I (*C*). *D*, same experiment as (*A*) except that HEK293T cells were stimulated after 24 h with 1000 IU/ml of IFN-β and expression of the luciferase reporter construct controlled by ISRE repeats (pISRE-Luc) was quantified 24 h later. *E and F*, PK15 cells were transfected with either the cytosolic DNA sensor ligand ISD (*E*) or poly(dA:dT) (*F*) together with pCI-neo-3xFLAG expression vectors encoding 3xFLAG alone or fused to A151R or MGF360-21R. After 36 h, the expression level of *IFN-β* was measured by RT-qPCR and normalized to that of *GAPDH*. Data are presented as a fold increase relative to the non-stimulated condition. *G and H*, Same conditions as (*A, B*) but with HEK293T cells knockdown BANF1 (si-BANF1) and control cells (si-NegC). All experiments were achieved in triplicate. Data represent means ± SD and are representative of three independent experiments. **, $p < 0.005$ and ***, $p < 0.0005$.

benzonase treatment (ASFV-infected, benzonase treatment). Similar to the previous AP-MS experiment, we compiled a list of background proteins to eliminate nonspecific binders (Supplemental Table S3*A*). We compared the protein identifications from the four datasets and identified several BANF1-protein interactions that were solely detected in either mock-infected or ASFV-infected cells (Fig. 8*A*). Notably, the number of DNA-dependent interactions unique to BANF1 was comparatively lower in infected cells than in non-infected cells. Term enrichment analysis of the proteins exclusively detected in mock-infected and infected cells highlighted their involvement in distinct cellular processes: regulation of chromatin remodeling (GO:0006338) and DNA replication (GO:0006260) in non-infected cells and nuclear transport (GO:0051168) and mRNA splicing (GO:0000398) in ASFV-infected cells (Fig. 8*B* and Supplemental Table S3*B*). Furthermore, we constructed a heatmap representing the BANF1 interactomes across various conditions (Fig. 8*C* and Supplemental Table S3*C*). A significant proportion of the high-confidence binding proteins play a role in diverse functions such as chromatin remodeling, transcription regulation, nuclear membrane organization, nuclear transport, and innate immune responses. Among these proteins, host factors that facilitate or hinder viral replication were present. In contrast to several ASFV proteins which co-purified with BANF1 exclusively in the presence of DNA, the interaction between BANF1 and A151R was detected even in the absence of DNA, confirming that DNA is not required and it is indeed a direct

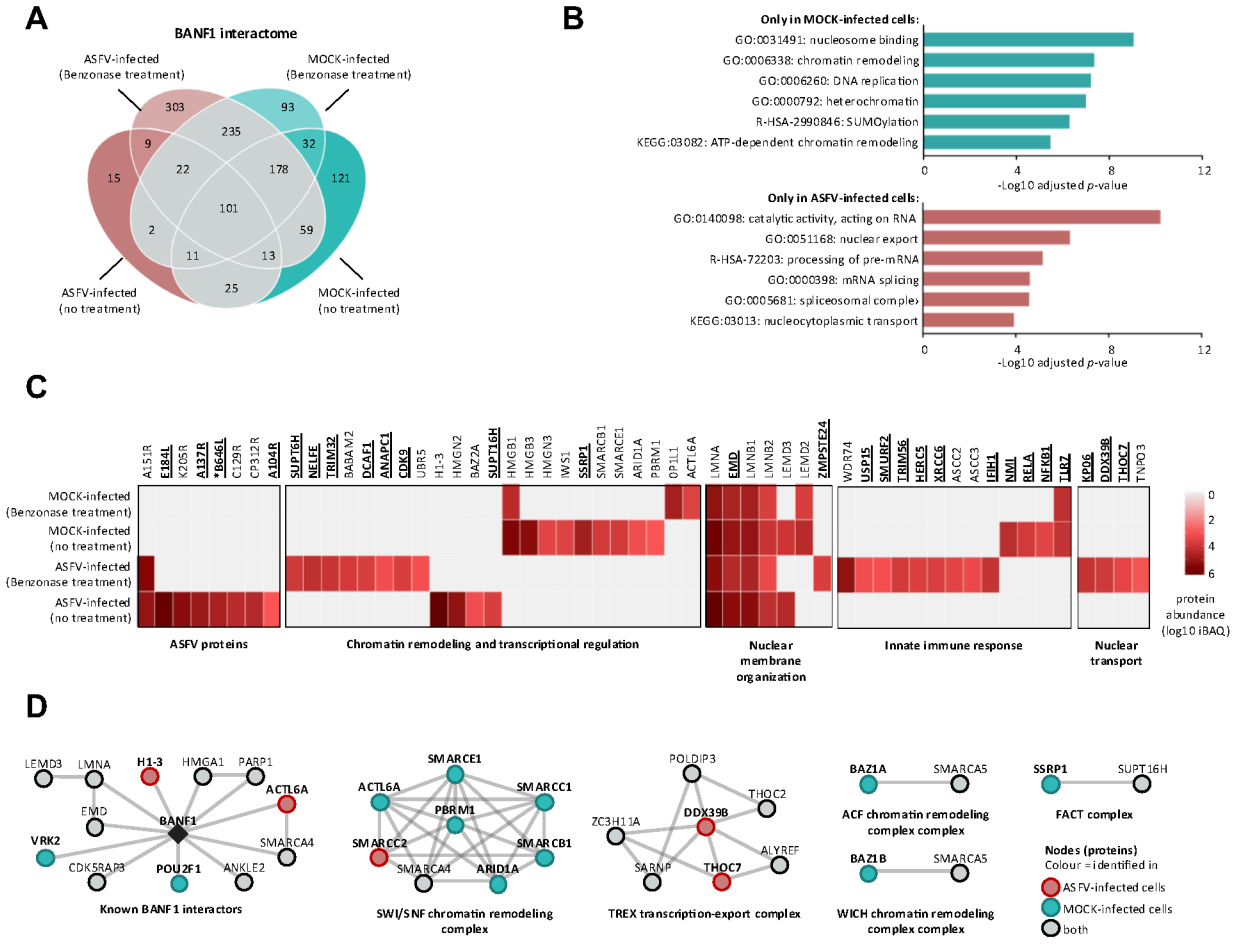

FIG. 8. **Comparison of the interactomes of BANF1 prepared from non-infected and ASFV-infected cells.** *A*, Venn diagram of proteins identified by AP-MS in WSL cells expressing BANF1-GFP, categorized by combinations of the infection status (mock or ASFV) and benzonase treatment (no or 25 U/ml benzonase). *B*, enrichment profiles of proteins interacting with BANF1 in mock-infected and ASFV-infected samples. The most significant GO, KEGG, and Reactome terms are shown with Benjamini-Hochberg FDR-corrected *p*-values. *C*, heatmap of high-confidence BANF1 interactors compared under different experimental conditions. Functional characterizations for grouped proteins are shown below the heatmap. Proteins known to be involved in virus replication (see references in Supplemental Table S3*C*) are highlighted in *bold* and *underlined*. ASFV proteins that are essential for virus replication are marked with an *asterisk* (*). *D*, the high-confidence proteins that bind to BANF1 were grouped into protein complexes according to the EBI Complex Portal and visualized with STRING to illustrate the experimentally validated protein-protein interaction among them. Node colors indicate the identification in ASFV-infected (*red*), mock-infected (*green*), or both (*grey* nodes) samples.

protein-protein interaction (PPI). Next, we concentrated on identifying the presence of established BANF1 interactors and protein complexes within our dataset (Fig. 8*D* and Supplemental Table S3*D*). Our data demonstrated that many interactions previously described between human BANF1 and other human proteins are also present in porcine cells. Additionally, in ASFV-infected cells, BANF1 interacted with actin-like protein 6A (ACTL6A) and histone H1.3. Conversely, the transcription factor POU2F1 and the serine/threonine-protein kinase (VRK2), responsible for phosphorylating BANF1, were exclusively identified in the absence of ASFV infection. Of the proteins not previously reported as BANF1 interactors, we noticed that those associated with various chromatin remodeling complexes and NFκB signaling pathway (RELA and NFκB1) were primarily identified in mock-infected samples. Moreover, RELA and NFκB1 were only detected in presence of DNA, suggesting that BANF1 could be recruited to the NFκB-responsive promoters and this complex is likely disrupted by ASFV. The binding of MDA5 and TLR7 indicates that BANF1 would also modulate IFN-I induction downstream of PRRs other than cGAS/STING. Interestingly, two components of the TREX transcription-export complex, the spliceosome RNA helicase (DDX39B) and THO complex subunit seven (THOC7), were exclusively identified in pulldowns from infected samples. Notably, the TREX complex was reported to be essential for exporting Kaposi's sarcoma-associated herpesvirus mRNA and virus replication (80).

Deletion of A151R or MGF360-21R Genes Increases IFN Responses in ASFV Infected cells

To further understand the role of *A151R* and *MGF360-21R* in the context of the viral infection of primary macrophages, two viruses with these single genes deleted (GeorgiaΔA151R and GeorgiaΔMGF360–21R) were purified as described in the experimental procedures section. Full genome sequencing confirmed that the deletions occurred at the expected genome positions: 49,653 to 50,107 for GeorgiaΔA151R and 187,834 to 188,782 for GeorgiaΔMGF360-21R (Fig. 9, *A* and *B*). The latter deletion leaves 267 bp of the *MGF360-21R* gene remaining (Fig. 9*B*), which avoided the concomitant deletion of the *nORF_187886* recently identified within the *MGF360-21R* gene (5). The remaining sequence could lead to the translation of a truncated protein. Indeed, upstream of the second ATG in this sequence there is a transcription start site that would produce a 61 amino acid protein (5). However, this protein is very unlikely to retain the function of the full length MGF360-21R. With the exception of a single T to A point mutation in the *E199L* gene that leads to a E125V mutation in pE199L in the GeorgiaΔA151R virus, no other mutations were observed as compared to the wild type virus. The ability of the recombinant viruses to replicate *in vitro,* was assessed over a multi-step growth curve (Fig. 9*C*). PBMs were infected with the deletion mutants or the wild type virus at a MOI of 0.01. Total virus from both cells and supernatants were collected at different times p.i. and titrated. All the viruses reached a plateau around 72 h p.i. with maximum titers of $10^{7.25}$ haemadsorbing dose 50% (HAD_{50}/ml) for WT and GeorgiaΔMGF360-21R and $10^{6.38}$ HAD_{50}/ml for GeorgiaΔA151R. Hence, the GeorgiaΔA151R mutant showed a growth defect, and this was most noticeable at 48 h p.i. ($p = 0.0009$). Given the impact of both proteins on the induction of type I IFN in transfected cells (Fig. 7), we evaluated the secretion of IFNα (Fig. 9*D*) and CXCL-10 (Fig. 9*E*), an interferon stimulated gene (ISG), by PBMs infected with WT or recombinant viruses. At 8 h post infection, supernatants from GeorgiaΔA151R infected cells contained significantly higher amounts of IFNα ($p = 0.0175$). At 16 h post infection, all supernatants contained substantial amounts of IFNα and again these were higher in GeorgiaΔA151R infected cells ($p < 0.0001$). A similar trend was observed for CXCL-10. At both 8 and 16 h post infection, CXCL-10 levels were significantly higher following infection with GeorgiaΔA151R ($p < 0.0001$). Notably, cells infected with GeorgiaΔMGF360-21R also secreted higher amounts of CXCL-10 than those infected with the wild type virus at 16 h p.i. ($p = 0.0028$). This indicates that MGF360-21R might have a smaller, but still significant, impact on the host IFN response.

DISCUSSION

Identifying virus–virus and virus–host PPIs provides important insights into molecular mechanisms of virus replication and pathogenesis. Over the past 2 decades, many novel PPIs involving ASFV proteins have been both experimentally identified (reviewed in reference (6), and in more recent studies (81–85)) and in one instance, even predicted using computational methods (86). However, about half of the currently annotated ASFV proteins still await characterization while the full panel of ASFV-coded proteins may not be completely determined yet (1, 5). Discovering new molecular virus-host interactions provides information about the functionality of so far uncharacterized viral proteins and cellular pathways involved in viral infection and pathogenesis and provides a basis for the rational development of antiviral drug targets and vaccines.

The starting point for this study was to investigate the potential functions of MGF360-21R, an uncharacterized protein within the ASFV MGF360. Previous research has shown that MGF360 and MGF505 members act as multifunctional immune-evasion proteins. They inhibit type I IFN responses by interacting with key proteins in the cGAS-STING and JAK-STAT (87–94) signaling pathways, often leading to their degradation. These results, however, are primarily based on targeted PPI studies focused on host proteins linked to immunity. This approach introduces a bias and leaves the specific host proteins, involved in regulation of other important pathways, unidentified. Here, we applied AP-MS and

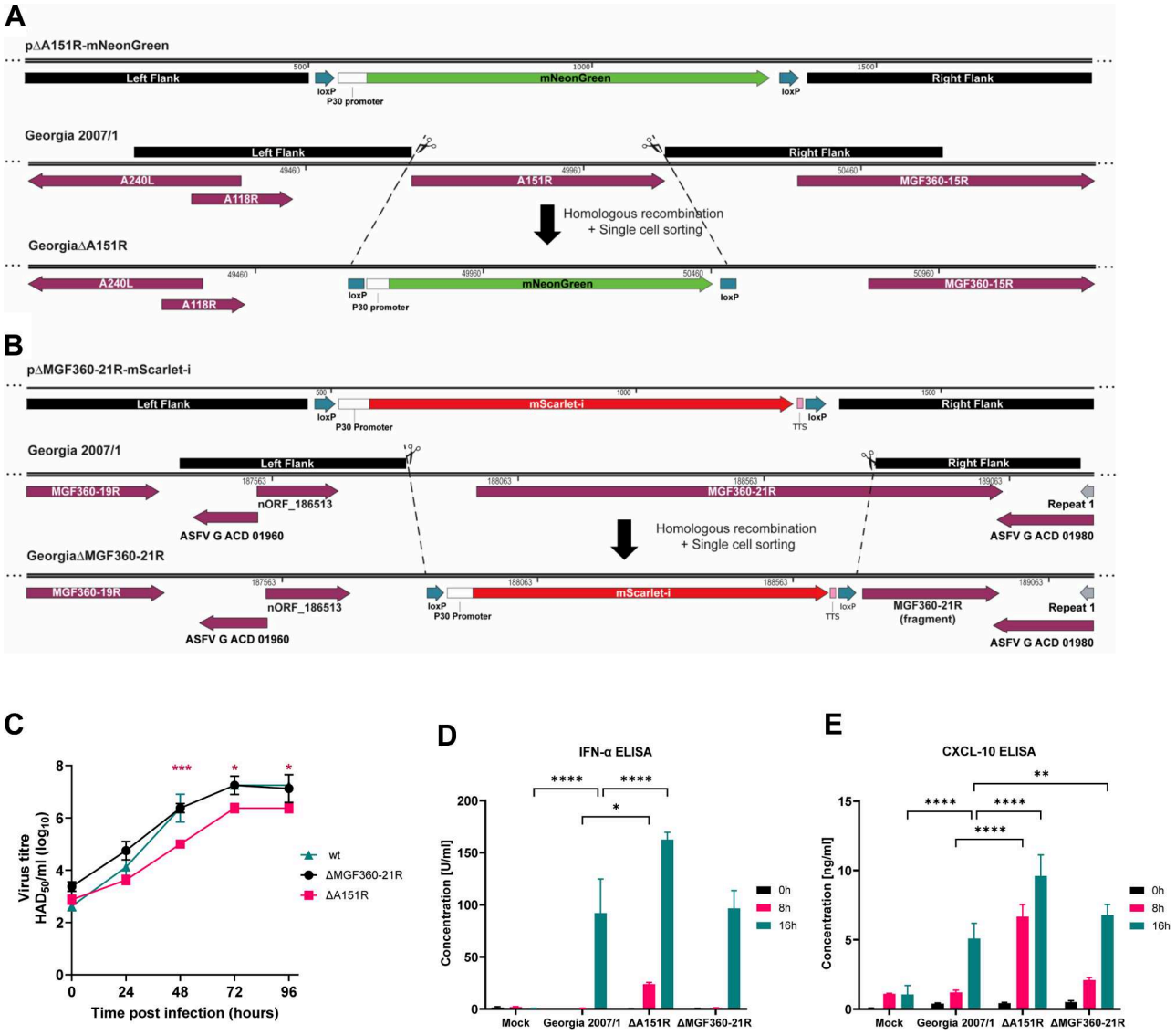

FIG. 9. **Purification, replication and IFN responses of ASFV GeorgiaΔA151R and GeorgiaΔMGF360-21R deletion mutants.** *A, B*, diagram showing plasmid constructs, sites of homologous recombination and final sequence of GeorgiaΔA151R and GeorgiaΔMGF360-21R deletion mutants respectively. *C*, multistep growth curves of the WT and gene-deleted viruses over a course of 4 days, where day 0 represents the inoculum. Means and standard deviations from two independent titrations are shown. Significant differences are represented by asterisks, where * is $p < 0.05$ and *** is $p < 0.001$. *D, E*, levels of IFN-α (D) and CXCL10 (E) from supernatants of purified PBMs infected with WT or recombinant viruses or mock infected. Means and standard deviations from duplicate measurements are shown. Significant differences, as compared with supernatants from wild type Georgia/2007 virus infected cells, are represented by asterisks, where * is $p < 0.05$, ** is $p < 0.01$ and **** is $p < 0.0001$.

Y2H, as "open-view" approaches, for the less biased identification of MGF360-21R interactors from the full complement of host and virus proteins present in an infected cell. It is noteworthy that expanding intra-viral PPI networks of viruses with a large genome like ASFV requires open-view proteomic techniques. While immunologic assays like immunoblots may be feasible to analyze PPI networks of smaller viruses, we had to consider a panel of at least 150 potential virus interactors and the fact that for many of them immunologic reagents are not available and even the expression of the corresponding ORF in mammalian cell culture is unclear. Interestingly, MGF360-21R was co-purified alongside another viral protein, pA151R, which has recently been recognized to inhibit IFN-β production (84, 95). Interactions between viral proteins can diversify targets inside the host cell and collectively influence its internal environment. Next, we focused on identifying potential interactions involving viral proteins pMGF360-21R and pA151R with host proteins.

We identified BANF1 as the high-confidence mutual interactor of ASFV MGF360-21R and A151R using AP-MS

(Fig. 1*E*) and Y2H screening (Fig. 2*B*). The observed interactions were subsequently validated through co-immunoprecipitation (Fig. 3) and colocalization studies (Fig. 4). Furthermore, MST experiments substantiated that the interaction between A151R and BANF1 is indeed direct (Fig. 3), which is an important finding considering that BANF1 is a known DNA-binding protein. We also demonstrated that the expression of either A151R or MGF360-21R leads to a relocalization of endogenous BANF1 from the nucleus to the cytoplasm. However, we were unable to detect the subcellular localization of BANF1 in the context of early ASFV infection despite no apparent degradation had been observed based on MS data and Western blot analyses. Thus, detection of BANF1 may have failed because critical epitopes detected by the anti-BANF1 monoclonal antibody might have been masked by post-translational modifications induced on BANF1 in response to the infection, thereby preventing recognition by the antibody. It is known that VV and HSV-1 infections can modulate the phosphorylation state of BANF1 (73, 74, 96, 97). Phosphorylation at the threonine and serine residues at positions 2, 3, and 4 by VKR kinases regulate BANF1 function (98, 99), particularly its DNA-binding affinity (29, 74, 100), and localization (77). In our studies we showed that the expression level of VRK1 is significantly increased in the absence of BANF1 (Fig. 6*F*), further investigations are warranted to determine whether ASFV could potentially influence the phosphorylation of BANF1 and its role in ASFV replication.

BANF1 is targeted by some viruses, which hijack its function for their replication. In our report, we demonstrated that BANF1 silencing led to greatly reduced viral titers suggesting a beneficial role of BANF1 in AFSV replication. The proviral function of BANF1 has already been described in the context of infection by various retroviruses such as HIV (Human Immunodeficiency Virus) or MoMLV (Moloney Murine Leukemia Virus), with BANF1 being part of their pre-integration complex (75, 101). In Gammaherpesviruses, including KSHV (Kaposi's Sarcoma-Associated Herpesvirus) and EBV (Epstein-Barr Virus), BANF1 facilitates lytic reactivation by inhibiting cGAS-mediated DNA sensing (102). Conversely, BANF1 can also exert an antiviral function in the replication of VV (96) and HSV-1 (74). This is achieved through its ability to bind their viral genome, thereby inhibiting genome replication.

BANF1 was originally discovered and named for its role in protecting retroviral DNA against suicidal autointegration (76). The DNA binding properties allow BANF1 to recognize and bind to dsDNA of both foreign (75, 103) and endogenous origin (27). Within the cytoplasm, BANF1 was shown to compete for DNA binding with cGAS (39), consequently restricting the cGAS-STING pathway and suppressing innate immune responses (104). These facts prompted us to investigate whether the interaction of pMGF360-21R and pA151R with BANF1 could regulate type I IFN induction during ASFV infection. While the expression of MGF360-21R and A151R have no effect on ISRE-luciferase gene expression in IFN-β-stimulated cells, they significantly inhibit the induction of IFN-α/β signaling downstream of cGAS/STING or RIG-I. Our findings correlate with a recent study showing the inhibitory effect of A151R on IFN-I induction (84, 95). Moreover, a *A151R* deletion mutant of the Georgia 2010 ASFV strain exhibits reduced virulence in domestic pigs and induces a protective response against experimental infection with its parental virulent strain (22). In our experiments, we have also shown that macrophages infected with a modified Georgia 2007/1 strain lacking *A151R* exhibit higher levels of IFN-α at 8 h and 16 h p.i. compared to those infected with the parental virulent Georgia 2007/1 strain (Fig. 9). Our findings not only confirm the crucial role of A151R in inhibiting the IFN-I pathway but also support previous observations showing similar significant difference in IFN-α/β production between avirulent/low virulent and high virulent ASFV strains (9, 38, 105–107). In contrast, the anti-IFN-I activity of MGF360-21R was revealed for the first time in this study, adding to other ASFV proteins belonging to the MGF (including MGF505–11R, MGF360–13L, MGF505-7R, MGF360–11L, MGF505-3R, MGF110-9L, MGF360-4L, MGF360–14L, MGF360–15R, and MGF505-2R) which have already been shown to inhibit IFN-I induction (37, 108–113). These genes have evolved through homologous recombination (114), which seems to be an effective mechanism employed by ASFV to generate genetic diversity and develop strategies to evade host immunity (7). Poxviruses seem to have evolved a similar mechanism, enabling them to adapt and to bypass host defenses despite their low mutation rate (115).

Although both MGF360-21R and A151R can impact IFN-I induction, this inhibition may occur independently of their interaction with BANF1. Conversely, suppression of BANF1 expression in porcine cells increases the expression of proteins linked to the innate immune response activation through the cGAS-STING and RIG-I pathway (Fig. 6*F*) and significantly reduces ASFV replication (Fig. 6*D*). Therefore, we cannot exclude the role of BANF1 in suppressing innate immune defenses. However, if BANF1 does not directly contribute to the inhibition of IFN-I by MGF360-21R and A151R, the question remains regarding the mechanism underlying this inhibition. Furthermore, we suggest that ASFV A151R could downregulate IFN-I signaling by acting as a transcriptional regulator, potentially suppressing the transcription of IFNs themselves and downstream IFN-regulated genes. During infection, protein pA151R is expressed in both the early and late stages (116) and has been observed to accumulate within the nucleus and the nuclear envelope (Fig. 4). The crystal structure of pA151R (21) revealed a Zn-binding site typically linked to interactions with DNA, RNA, and with various proteins (117). We hypothesize that pA151R might modulate gene transcription through direct or indirect interactions with nucleic acids. Like EBV's Zta protein (118), pA151R could recognize and bind directly to specific DNA sequences within

the host genome. On the other hand, many viral transcriptional regulators only bind DNA when in complex with host transcription factors. This characteristic could also apply to pA151R and will require additional investigations.

As more functional studies appear, it becomes clear that ASFV proteins have the potential to display moonlighting characteristics, meaning their functions can vary due to alterations in cellular localization, infection stages, cell types, or changes in the concentration of a cellular or viral ligand. We demonstrated the inhibitory role of ASFV proteins pMGF360-21R and pA151R in IFN-I signaling. Nonetheless, both proteins might perform additional functions attributed to their interaction with BANF1. Given the high expression of pA151R and pMGF360-21R within 2 to 6 h p.i., it is highly likely that both proteins have substantial roles in the early phase of infection. Previous studies indicate that within the initial 4 h of infection, ASFV triggers the formation of nuclear blebs (119) and disrupts the lamina network, releasing nuclear material into the cytoplasm (120). The nuclear lamina is a filamentous meshwork forming an interface between the inner nuclear membrane and the peripheral chromatin. BANF1 is an integral component of the lamina network, which is essential for nuclear envelope assembly (121). Therefore, further investigations are needed to assess whether the interaction with BANF1 (i) contributes to the disruption of the lamina network caused by ASFV, and (ii) facilitates the transport of viral DNA and proteins between the nucleus and cytoplasm, enhancing viral replication.

DATA AVAILABILITY

All MS raw data and MaxQuant output tables were deposited in the ProteomeXchange Consortium (http://proteomecentral.proteomexchange.org) via the PRIDE partner repository (122) with the dataset identifier PXD047794.

Supplemental Data—This article contains supplemental data as referenced in Supplemental Figure S1 and Supplementary Tables S1, *A–E*, S2 and S3, *A–D* (70, 71).

Acknowledgments—We thank the Biobank of the Friedrich-Loeffler-Institut for providing the WSL cell line. We also thank Dr Pierre-Olivier Vidalain, Dr Axel Grot, Dr Marion Sourisseau, Sarah Thibaudeau and Barbara Bettin for the fruitful discussions and their technical assistance.

Author Contributions—C. L. N., L. K. D., A. L. R., D. V., M. L. P., A. K., G. C., J. D., K. M. D., and G. P. conceptualization; C. L. N., L. K. D., A. L. R., D. V., M. L. P., A. K., G. C., J. D., K. M. D., G. P., A. M., L. C. G., R. K., T. K. S., J. B. B., A. F., M. L. D., and G. K. methodology; C. L. N., L. K. D., A. L. R., D. V., M. L. P., A. K., G. C., J. D., K. M. D., G. P., A. M., L. C. G., R. K., T. K. S., J. B. B., A. F., M. L. D., and G. K. validation; C. L. N., L. K. D., A. L. R., D. V., M. L. P., A. K., G. C., J. D., K. M. D., and G. P. formal analysis; C. L. N., L. K. D., A. L. R., D. V., M. L. P., A. K., G. C., J. D., K. M. D., G. P., A. M., L. C. G., R. K., T. K. S., J. B. B., A. F., M. L. D., and G. K. investigation; C. L. N., L. K. D., A. L. R., D. V., M. L. P., A. K., G. C., J. D., K. M. D., G. P., A. M., L. C. G., R. K., T. K. S., J. B. B., A. F., M. L. D., and G. K. resources; C. L. N., L. K. D., A. L. R., D. V., M. L. P., A. K., G. C., J. D., K. M. D., and G. P. writing–original draft; C. L. N., L. K. D., A. L. R., D. V., M. L. P., A. K., G. C., J. D., K. M. D., and G. P. writing–review & editing; C. L. N., L. K. D., A. L. R., D. V., M. L. P., A. K., G. C., J. D., K. M. D., and G. P. visualization; C. L. N., L. K. D., A. L. R., D. V., M. L. P., A. K., G. C., and J. B. B. supervision; C. L. N., L. K. D., A. L. R., D. V., M. L. P., A. K., G. C., and J. B. B. project administration; C. L. N., L. K. D., A. L. R., D. V., M. L. P., A. K., and G. C. funding acquisition; E. H. software.

Funding and Additional Information—This work was supported by research grants from European Commission, Horizon 2020 Framework Program European Union ERA- NET project ASFVInt, grant agreement 862605, and FLI's ASFV Research Network. The project ASFVInt was made also possible by co-funding, under the grant codes: ANR-21-ICRD-0001-01 for ANSES and ANR-21-ICRD-0001 to 02 for INRAE. J.D. is supported by a PhD fellowship from ANSES and INRAE. A. M., L. C. G., C. L. N., L. K. D., A. L. R. were supported by UKRI grants BBS/E/I/00007034, BBS/E/I/00007037, BBS/E/PI/0000230002B, and BBS/E/PI/000023NB0004. Work in the Bosse lab was funded by the Deutsche Forschungsgemeinschaft (DFG, German Research Foundation) under the Germany's Excellence Strategy EXC 2155—project no. 390874280, the RTG 2771 Humans and Microbes project no. 453548970, and the RTG 2887 VISION project number 49735088 project BO 4158/5-1 as well as the Wellcome Trust through a Collaborative Award (209250/Z/17/Z). The funders had no role in study design, data collection and analysis, decision to publish, or preparation of the manuscript.

Conflict of Interest—The authors declare that they do not have any conflicts of interest with the content of this article.

Abbreviations—The abbreviations used are: 3-AT, 3-aminotriazole; ACTL6A, actin-like protein 6A; ANOVA, two-way analysis of variance; AP-MS, affinity tag purification-mass spectrometry; ASFV, African Swine Fever Virus; BANF1, barrier-to-autointegration factor 1; BSA, bovine serum albumin; cGAS, Cyclic GMP-AMP synthase; COX2, cytochrome c oxidase subunit 2; CRAPome, Contaminant Repository for Affinity Purification; EBV, Epstein-Barr Virus; ECL, enhanced chemiluminescence; ELOB, elongin B; ELOC, elongin C; FA, formic acid; FACS, fluorescence-activated cell sorting; FASP, Filter-aided sample preparation; FBS, fetal bovine serum; Fc, fold change; FDR, false discovery rates; Gal4-AD, Gal4 transactivation domain; Gal4-BD, Gal4 DNA-

binding domain; GFP, green fluorescent protein; GO, gene ontology; h, hours; HAD_{50}/ml, hemadsorbing dose 50%; HIV, Human Immunodeficiency Virus; HT-Y2H, high-throughput yeast two-hybrid; HSV-1, Herpes Simplex Virus 1; IFN-I or IFN-α/β, type I interferon; IMDM, Iscove's modified Dulbecco's medium; ISD, interferon stimulated DNA; IL17RA, interleukin-17 receptor A; ISG, interferon stimulated gene; ISRE, IFN-stimulated response element; K_d, dissociation constant; kDa, kilodaltons; KEGG, Kyoto Encyclopedia of Genes and Genomes; KSHV, Kaposi's Sarcoma-Associated Herpesvirus; LFQ, label-free quantitation values; MGF, multigene family; MOI, multiplicity of infection; MoMLV, Moloney Murine Leukemia Virus; MST, microscale thermophoresis; NA, not available; NΔRIG-I, N-terminal CARDs of RIG-I; NT, non-transfected; ORF, open reading frame; PAE, predicted aligned error; PAM, porcine alveolar macrophages; PBMs, porcine bone marrow cells; PBS, phosphate-buffered saline; PFA, paraformaldehyde; p.i., post infection; PPI, protein-protein interaction; PRRs, pattern recognition receptors; PYCR, pyrroline-5-carboxylate reductases; RPMI, Roswell Park Memorial Institute; RPS15, small ribosomal subunit protein uS19; SDS-PAGE, SDS-polyacrylamide gel electrophoresis; si-NegC, nonspecific siRNA; siRNA, short interfering RNA; STING, Cyclic GMP-AMP/Stimulator of interferon genes; TBST, Tris-buffered saline with 0.25% Tween-20; $TCID_{50}$, 50% tissue culture infective doses; TFPT, TCF3 fusion partner; THOC7, THO complex subunit 7; TMB, 3,3′,5,5′-tetramethylbenzidine; VRK1, vaccinia-related kinase 1; TUBB, tubulin beta chain; VV, vaccinia virus; WOAH, World Organization for Animal Health; WSL, wild boar lung-derived cells; ZMPSTE24, zinc metalloproteinase Ste24 homolog.

Received May 5, 2025, and in revised form, July 2, 2025 Published, MCPRO Papers in Press, July 22, 2025, https://doi.org/10.1016/j.mcpro.2025.101038

REFERENCES

1. Wöhnke, E., Cackett, G., Werner, F., Blome, S., Mettenleiter, T. C., and Karger, A. (2022) Proteome analysis of swine macrophages after infection with two genotype II african swine fever isolates of different pathogenicity. *Viruses* **14**, 2140
2. Keßler, C., Forth, J. H., Keil, G. M., Mettenleiter, T. C., Blome, S., and Karger, A. (2018) The intracellular proteome of African swine fever virus. *Sci. Rep.* **8**, 14714
3. Wöhnke, E., Fuchs, W., Hartmann, L., Blohm, U., Blome, S., Mettenleiter, T. C., *et al*. (2021) Comparison of the proteomes of porcine macrophages and a stable porcine cell line after infection with african swine fever virus. *Viruses* **13**, 2198
4. Alejo, A., Matamoros, T., Guerra, M., and Andrés, G. (2018) A proteomic Atlas of the African swine fever virus particle. *J. Virol.* **92**. https://doi.org/10.1128/jvi.01293-18
5. Cackett, G., Portugal, R., Matelska, D., Dixon, L., and Werner, F. (2022) African swine fever virus and host response: transcriptome profiling of the Georgia 2007/1 strain and porcine macrophages. *J. Virol.* **96**, e01939-21
6. Dolata, K. M., Pei, G., Netherton, C. L., and Karger, A. (2023) Functional landscape of African swine fever virus–host and virus–virus protein interactions. *Viruses* **15**, 1634
7. Zhu, Z., Xiao, C.-T., Fan, Y., Cai, Z., Lu, C., Zhang, G., *et al*. (2019) Homologous recombination shapes the genetic diversity of African swine fever viruses. *Vet. Microbiol.* **236**, 108380
8. O'Donnell, V., Holinka, L. G., Gladue, D. P., Sanford, B., Krug, P. W., Lu, X., *et al*. (2015) African swine fever virus Georgia isolate harboring deletions of MGF360 and MGF505 genes is attenuated in swine and confers protection against challenge with virulent parental virus. *J. Virol.* **89**, 6048–6056
9. Reis, A. L., Abrams, C. C., Goatley, L. C., Netherton, C., Chapman, D. G., Sanchez-Cordon, P., *et al*. (2016) Deletion of African swine fever virus interferon inhibitors from the genome of a virulent isolate reduces virulence in domestic pigs and induces a protective response. *Vaccine* **34**, 4698–4705
10. Boinas, F. S., Hutchings, G. H., Dixon, L. K., and Wilkinson, P. J. (2004) Characterization of pathogenic and non-pathogenic African swine fever virus isolates from Ornithodoros erraticus inhabiting pig premises in Portugal. *J. Gen. Virol.* **85**, 2177–2187
11. Dixon, L. K., Chapman, D. A. G., Netherton, C. L., and Upton, C. (2013) African swine fever virus replication and genomics. *Virus Res.* **173**, 3–14
12. Chapman, D. A. G., Tcherepanov, V., Upton, C., and Dixon, L. K. (2008) Comparison of the genome sequences of non-pathogenic and pathogenic African swine fever virus isolates. *J. Gen. Virol.* **89**, 397–408
13. Burrage, T. G., Lu, Z., Neilan, J. G., Rock, D. L., and Zsak, L. (2004) African swine fever virus multigene family 360 genes affect virus replication and generalization of infection in Ornithodoros porcinus ticks. *J. Virol.* **78**, 2445–2453
14. Ding, M., Dang, W., Liu, H., Xu, F., Huang, H., Sunkang, Y., *et al*. (2022) Combinational deletions of MGF360-9L and MGF505-7R attenuated highly virulent African swine fever virus and conferred protection against homologous challenge. *J. Virol.* **96**, e00329-22
15. Zsak, L., Lu, Z., Burrage, T. G., Neilan, J. G., Kutish, G. F., Moore, D. M., *et al*. (2001) African swine fever virus multigene family 360 and 530 genes are novel macrophage host range determinants. *J. Virol.* **75**, 3066–3076
16. Yang, K., Xue, Y., Niu, H., Shi, C., Cheng, M., Wang, J., *et al*. (2022) African swine fever virus MGF360-11L negatively regulates cGAS-STING-mediated inhibition of type I interferon production. *Vet. Res.* **53**, 7
17. Zhuo, Y., Guo, Z., Ba, T., Zhang, C., He, L., Zeng, C., *et al*. (2020) African swine fever virus MGF360-12L inhibits type I interferon production by blocking the interaction of importin α and NF-κB signaling pathway. *Virol. Sin.* **36**, 176–186
18. Wang, Y., Cui, S., Xin, T., Wang, X., Yu, H., Chen, S., *et al*. (2022) African swine fever virus MGF360-14L negatively regulates type I interferon signaling by targeting IRF3. *Front. Cell Infect. Microbiol.* **11**, 818969
19. Luo, J., Cheng, M., Duan, Y., Xing, X., Lu, M., Sun, Y., *et al*. (2023) African swine fever virus encoded protein MGF360-13L inhibits cGAS-STING-mediated IFN-I signaling pathway. *Gene* **874**, 147490
20. Wang, Z., He, Y., Huang, Y., Zhai, W., Tao, C., Chu, Y., *et al*. (2024) African swine fever virus MGF360-4L protein attenuates type I interferon response by suppressing the phosphorylation of IRF3. *Front. Immunol.* **15**, 1382675
21. Huang, J.-W., Niu, D., Liu, K., Wang, Q., Ma, L., Chen, C.-C., *et al*. (2020) Structure basis of non-structural protein pA151R from African swine fever virus. *Biochem. Biophys. Res. Commun.* **532**, 108–113
22. Ramirez-Medina, E., Vuono, E., Pruitt, S., Rai, A., Espinoza, N., Valladares, A., *et al*. (2022) ASFV gene A151R is involved in the process of virulence in domestic swine. *Viruses* **14**, 1834
23. Gorjánácz, M., Klerkx, E. P., Galy, V., Santarella, R., López-Iglesias, C., Askjaer, P., *et al*. (2007) Caenorhabditis elegans BAF-1 and its kinase VRK-1 participate directly in post-mitotic nuclear envelope assembly. *EMBO J.* **26**, 132–143
24. Haraguchi, T., Koujin, T., Segura-Totten, M., Lee, K. K., Matsuoka, Y., Yoneda, Y., *et al*. (2001) BAF is required for emerin assembly into the reforming nuclear envelope. *J. Cell Sci.* **114**, 4575–4585
25. Haraguchi, T., Kojidani, T., Koujin, T., Shimi, T., Osakada, H., Mori, C., *et al*. (2008) Live cell imaging and electron microscopy reveal dynamic processes of BAF-directed nuclear envelope assembly. *J. Cell Sci.* **121**, 2540–2554
26. Asencio, C., Davidson, I. F., Santarella-Mellwig, R., Ly-Hartig, T. B. N., Mall, M., Wallenfang, M. R., *et al*. (2012) Coordination of kinase and phosphatase activities by Lem4 enables nuclear envelope reassembly during mitosis. *Cell* **150**, 122–135
27. Samwer, M., Schneider, M. W. G., Hoefler, R., Schmalhorst, P. S., Jude, J. G., Zuber, J., *et al*. (2017) DNA cross-bridging shapes a single nucleus from a set of mitotic chromosomes. *Cell* **170**, 956–972.e23

28. Young, A. M., Gunn, A. L., and Hatch, E. M. (2020) BAF facilitates interphase nuclear membrane repair through recruitment of nuclear transmembrane proteins. *Mol. Biol. Cell* **31**, 1551–1560
29. Halfmann, C. T., Sears, R. M., Katiyar, A., Busselman, B. W., Aman, L. K., Zhang, Q., *et al*. (2019) Repair of nuclear ruptures requires barrier-to-autointegration factor. *J. Cell Biol.* **218**, 2136–2149
30. Montes de Oca, R., Shoemaker, C. J., Gucek, M., Cole, R. N., and Wilson, K. L. (2009) Barrier-to-Autointegration factor proteome reveals chromatin-regulatory partners. *PLoS One* **4**, e7050
31. Bolderson, E., Burgess, J. T., Li, J., Gandhi, N. S., Boucher, D., Croft, L. V., *et al*. (2019) Barrier-to-autointegration factor 1 (Banf1) regulates poly [ADP-ribose] polymerase 1 (PARP1) activity following oxidative DNA damage. *Nat. Commun.* **10**, 5501
32. Wang, X., Xu, S., Rivolta, C., Li, L. Y., Peng, G.-H., Swain, P. K., *et al*. (2002) Barrier to autointegration factor interacts with the cone-rod homeobox and represses its transactivation function. *J. Biol. Chem.* **277**, 43288–43300
33. Margalit, A., Neufeld, E., Feinstein, N., Wilson, K. L., Podbilewicz, B., and Gruenbaum, Y. (2007) Barrier to autointegration factor blocks premature cell fusion and maintains adult muscle integrity in C. elegans. *J. Cell Biol.* **178**, 661–673
34. Sears, R. M., and Roux, K. J. (2020) Diverse cellular functions of barrier-to-autointegration factor and its roles in disease. *J. Cell Sci.* **133**, jcs246546
35. He, W.-R., Yuan, J., Ma, Y.-H., Zhao, C.-Y., Yang, Z.-Y., Zhang, Y., *et al*. (2022) Modulation of host antiviral innate immunity by African swine fever virus: a review. *Animals* **12**, 2935
36. Ayanwale, A., Trapp, S., Guabiraba, R., Caballero, I., and Roesch, F. (2022) New insights in the interplay between African swine fever virus and innate immunity and its impact on viral pathogenicity. *Front Microbiol.* **13**, 958307
37. Afe, A. E., Shen, Z.-J., Guo, X., Zhou, R., and Li, K. (2023) African swine fever virus interaction with host innate immune factors. 6. *Viruses* **15**, 1220
38. García-Belmonte, R., Pérez-Núñez, D., Pittau, M., Richt, J. A., and Revilla, Y. (2019) African swine fever virus Armenia/07 virulent strain controls interferon beta production through the cGAS-STING pathway. *J. Virol.* **93**, e02298
39. Guey, B., Wischnewski, M., Decout, A., Makasheva, K., Kaynak, M., Sakar, M. S., *et al*. (2020) BAF restricts cGAS on nuclear DNA to prevent innate immune activation. *Science* **369**, 823–828
40. Keil, G. M., Giesow, K., and Portugal, R. (2014) A novel bromodeoxyuridine-resistant wild boar lung cell line facilitates generation of African swine fever virus recombinants. *Arch. Virol.* **159**, 2421–2428
41. Hübner, A., Keil, G. M., Kabuuka, T., Mettenleiter, T. C., and Fuchs, W. (2018) Efficient transgene insertion in a pseudorabies virus vector by CRISPR/Cas9 and marker rescue-enforced recombination. *J. Virol. Methods* **262**, 38–47
42. Hübner, A., Petersen, B., Keil, G. M., Niemann, H., Mettenleiter, T. C., and Fuchs, W. (2018) Efficient inhibition of African swine fever virus replication by CRISPR/Cas9 targeting of the viral p30 gene (CP204L). *Sci. Rep.* **8**, 1449
43. REED, L. J., and MUENCH, H. (1938) A simple method of estimating fifty per cent ENDPOINTS12. *Am. J. Epidemiol.* **27**, 493–497
44. Tyanova, S., Temu, T., Sinitcyn, P., Carlson, A., Hein, M. Y., Geiger, T., *et al*. (2016) The Perseus computational platform for comprehensive analysis of (prote)omics data. *Nat. Methods* **13**, 731–740
45. Mellacheruvu, D., Wright, Z., Couzens, A. L., Lambert, J.-P., St-Denis, N. A., Li, T., *et al*. (2013) The CRAPome: a contaminant repository for affinity purification–mass spectrometry data. *Nat. Methods* **10**, 730–736
46. Dolata, K. M., Fuchs, W., Caignard, G., Dupré, J., Pannhorst, K., Blome, S., *et al*. (2023) CP204L is a multifunctional protein of African swine fever virus that interacts with the VPS39 subunit of the homotypic fusion and vacuole protein sorting complex and promotes lysosome clustering. *J. Virol.* **97**, e01943-22
47. Wiśniewski, J. R., Zougman, A., Nagaraj, N., and Mann, M. (2009) Universal sample preparation method for proteome analysis. *Nat. Methods* **6**, 359–362
48. Dyer, S. C., Austine-Orimoloye, O., Azov, A. G., Barba, M., Barnes, I., Barrera-Enriquez, V. P., *et al*. (2024) Ensembl 2025. *Nucleic Acids Res.* **53**, D948–D957
49. Sayers, E. W., Beck, J., Bolton, E. E., Brister, J. R., Chan, J., Connor, R., *et al*. (2024) Database resources of the national center for Biotechnology information in 2025. *Nucleic Acids Res.* **53**, D20–D29
50. Cox, J., and Mann, M. (2008) MaxQuant enables high peptide identification rates, individualized p.p.b.-range mass accuracies and proteome-wide protein quantification. *Nat. Biotechnol.* **26**, 1367–1372
51. Kolberg, L., Raudvere, U., Kuzmin, I., Vilo, J., and Peterson, H. (2020) gprofiler2 – an R package for gene list functional enrichment analysis and namespace conversion toolset g:Profiler. *F1000Res.* **9**, ELIXIR-709
52. Lieberman, P. M. (2008) Chromatin organization and virus gene expression. *J. Cell Physiol.* **216**, 295–302
53. Sayols, S. (2023) rrvgo: a Bioconductor package for interpreting lists of Gene Ontology terms. *Micropubl. Biol.* https://doi.org/10.17912/micropub.biology.000811
54. Shannon, P., Markiel, A., Ozier, O., Baliga, N. S., Wang, J. T., Ramage, D., *et al*. (2003) Cytoscape: a software environment for integrated models of biomolecular interaction networks. *Genome Res.* **13**, 2498–2504
55. Doncheva, N. T., Morris, J. H., Holze, H., Kirsch, R., Nastou, K. C., Cuesta-Astroz, Y., *et al*. (2023) Cytoscape stringApp 2.0: analysis and visualization of heterogeneous biological networks. *J. Proteome Res.* **22**, 637–646
56. Vidalain, P.-O., Jacob, Y., Hagemeijer, M. C., Jones, L. M., Neveu, G., Roussarie, J.-P., *et al*. (2014) A field-proven yeast two-hybrid protocol used to identify coronavirus–host protein–protein interactions. *Coronaviruses* **1282**, 213–229
57. Fablet, A., Kundlacz, C., Dupré, J., Hirchaud, E., Postic, L., Sailleau, C., *et al*. (2022) Comparative virus-host protein interactions of the bluetongue virus NS4 virulence factor. *Viruses* **14**, 182
58. Pei, G., Zyla, J., He, L., Moura-Alves, P., Steinle, H., Saikali, P., *et al*. (2021) Cellular stress promotes NOD1/2-dependent inflammation via the endogenous metabolite sphingosine-1-phosphate. *EMBO J.* **40**, e106272
59. Laemmli, U. K. (1970) Cleavage of structural proteins during the assembly of the head of bacteriophage T4. *Nature* **227**, 680–685
60. Towbin, H., Staehelin, T., and Gordon, J. (1979) Electrophoretic transfer of proteins from polyacrylamide gels to nitrocellulose sheets: procedure and some applications. *Proc. Natl. Acad. Sci.* **76**, 4350–4354
61. Schneider, C. A., Rasband, W. S., and Eliceiri, K. W. (2012) NIH Image to ImageJ: 25 years of image analysis. *Nat. Methods* **9**, 671–675
62. Mirdita, M., Schütze, K., Moriwaki, Y., Heo, L., Ovchinnikov, S., and Steinegger, M. (2022) ColabFold: making protein folding accessible to all. *Nat. Methods* **19**, 679–682
63. [Preprint] Evans, R., O'Neill, M., Pritzel, A., Antropova, N., Senior, A., Green, T., *et al*. (2021) Protein complex prediction with AlphaFold-Multime. *bioRxiv*. https://doi.org/10.1101/2021.10.04.463034
64. Rathakrishnan, A., Moffat, K., Reis, A. L., and Dixon, L. K. (2020) Production of recombinant African swine fever viruses: speeding up the process. 6. *Viruses* **12**, 615
65. Goatley, L. C., Freimanis, G., Tennakoon, C., Foster, T. J., Quershi, M., Dixon, L. K., *et al*. (2024) Full genome sequence analysis of African swine fever virus isolates from Cameroon. *PLoS One* **19**, e0293049
66. Chapman, D. A. G., Darby, A. C., Da Silva, M., Upton, C., Radford, A. D., and Dixon, L. K. (2011) Genomic analysis of highly virulent Georgia 2007/1 isolate of African swine fever virus. *Emerg. Infect Dis.* **17**, 599–605
67. Ashburner, M., Ball, C. A., Blake, J. A., Botstein, D., Butler, H., Cherry, J. M., *et al*. (2000) Gene Ontology: tool for the unification of biology. *Nat. Genet.* **25**, 25–29
68. Kanehisa, M., and Goto, S. (2000) KEGG: Kyoto Encyclopedia of genes and genomes. *Nucleic Acids Res.* **28**, 27–30
69. Jassal, B., Matthews, L., Viteri, G., Gong, C., Lorente, P., Fabregat, A., *et al*. (2020) The reactome pathway knowledgebase. *Nucleic Acids Res.* **48**, D498–D503
70. Szklarczyk, D., Franceschini, A., Wyder, S., Forslund, K., Heller, D., Huerta-Cepas, J., *et al*. (2015) STRING v10: protein–protein interaction networks, integrated over the tree of life. *Nucleic Acids Res.* **43**, D447
71. Meldal, B. H. M., Forner-Martinez, O., Costanzo, M. C., Dana, J., Demeter, J., Dumousseau, M., *et al*. (2015) The complex portal - an encyclopaedia of macromolecular complexes. *Nucleic Acids Res.* **43**, D479–D484
72. Cai, M., Huang, Y., Zheng, R., Wei, S. Q., Ghirlando, R., Lee, M. S., *et al*. (1998) Solution structure of the cellular factor BAF responsible for protecting retroviral DNA from autointegration. *Nat. Struct. Biol.* **5**, 903–909

73. Ibrahim, N., Wicklund, A., and Wiebe, M. S. (2011) Molecular characterization of the host defense activity of the barrier to autointegration factor against vaccinia virus. *J. Virol.* **85**, 11588–11600
74. Jamin, A., Thunuguntla, P., Wicklund, A., Jones, C., and Wiebe, M. S. (2014) Barrier to autointegration factor becomes dephosphorylated during HSV-1 infection and can act as a host defense by impairing viral DNA replication and gene expression. *PLoS One* **9**, e100511
75. Lee, M. S., and Craigie, R. (1998) A previously unidentified host protein protects retroviral DNA from autointegration. *Proc. Natl. Acad. Sci.* **95**, 1528–1533
76. Jacque, J.-M., and Stevenson, M. (2006) The inner-nuclear-envelope protein emerin regulates HIV-1 infectivity. *Nature* **441**, 641–645
77. Nichols, R. J., Wiebe, M. S., and Traktman, P. (2006) The vaccinia-related kinases phosphorylate the N′ terminus of BAF, regulating its interaction with DNA and its retention in the nucleus. *Mol. Biol. Cell* **17**, 2451–2464
78. Navarro, C. L., Cadiñanos, J., Sandre-Giovannoli, A. D., Bernard, R., Courrier, S., Boccaccio, I., *et al*. (2005) Loss of ZMPSTE24 (FACE-1) causes autosomal recessive restrictive dermopathy and accumulation of Lamin A precursors. *Hum. Mol. Genet.* **14**, 1503–1513
79. Capanni, C., Del Coco, R., Mattioli, E., Camozzi, D., Columbaro, M., Schena, E., *et al*. (2009) Emerin—prelamin A interplay in human fibroblasts. *Biol. Cell* **101**, 541–554
80. Boyne, J. R., Colgan, K. J., and Whitehouse, A. (2008) Recruitment of the Complete hTREX complex is required for kaposi's sarcoma–associated herpesvirus intronless mRNA nuclear export and virus replication. *PLoS Pathog.* **4**, e1000194
81. Shi, M., Zhou, N., Xiu, M., Li, X., Shan, F., Chen, W., *et al*. (2024) Identification of host proteins that interact with African swine fever virus pE301R. *Eng. Microbiol.* **4**, 100149
82. Wang, Z., Wang, Y., Zhao, P., Cui, S., Tao, C., Huang, Y., *et al*. (2025) DNAJA3 interacts with ASFV MGF360-14 L protein and reduces MGF360-14 L antagonistic role on Beta interferon production. *Int. J. Biol. Macromol* **310**, 143159
83. Chu, X., Ge, S., Wu, B., Zuo, Y., Xu, T., Yu, J., *et al*. (2025) ASFV p30 interacts with CCAR2 and MATR3 to promote ASFV replication. *Vet. Microbiol.* **302**, 110416
84. Wu, Q., Lei, Y., Zuo, Y., Zhang, J., Guo, F., Xu, W., *et al*. (2023) Interactome between ASFV and host immune pathway proteins. *mSystems* **8**, e00471-23
85. Weng, Z., Zheng, X., Liang, Y., Chen, X., Peng, Q., Zhang, G., *et al*. (2024) Porcine alveolar macrophages host proteins interacting with African swine fever virus p72. *Front. Microbiol.* **15**, 1370417
86. Fenster, J. A., Azzinaro, P. A., Dinhobl, M., Borca, M. V., Spinard, E., and Gladue, D. P. (2024) African swine fever virus protein–protein interaction prediction. *Viruses* **16**, 1170
87. Li, D., Peng, J., Wu, J., Yi, J., Wu, P., Qi, X., *et al*. (2023) African swine fever virus MGF-360-10L is a novel and crucial virulence factor that mediates ubiquitination and degradation of JAK1 by recruiting the E3 ubiquitin ligase HERC5. *mBio* **14**, e00606–e00623
88. Li, D., Zhang, J., Yang, W., Li, P., Ru, Y., Kang, W., *et al*. (2021) African swine fever virus protein MGF-505-7R promotes virulence and pathogenesis by inhibiting JAK1- and JAK2-mediated signaling. *J. Biol. Chem.* **297**, 101190
89. Zhang, K., Yang, B., Shen, C., Zhang, T., Hao, Y., Zhang, D., *et al*. (2022) MGF360-9L is a major virulence factor associated with the African swine fever virus by antagonizing the JAK/STAT signaling pathway. *mBio* **13**, e02330-21
90. Cheng, M., Luo, J., Duan, Y., Yang, Y., Shi, C., Sun, Y., *et al*. (2022) African swine fever virus MGF505-3R inhibits cGAS-STING-mediated IFN-β pathway activation by degrading TBK1. *Anim. Dis.* **2**, 13
91. Yang, K., Huang, Q., Wang, R., Zeng, Y., Cheng, M., Xue, Y., *et al*. (2021) African swine fever virus MGF505-11R inhibits type I interferon production by negatively regulating the cGAS-STING-mediated signaling pathway. *Vet. Microbiol.* **263**, 109265
92. Yang, K., Xue, Y., Niu, T., Li, X., Cheng, M., Bao, M., *et al*. (2022) African swine fever virus MGF505-7R protein interacted with IRF7and TBK1 to inhibit type I interferon production. *Virus Res.* **322**, 198931
93. Dupré, J., Le Dimna, M., Hutet, E., Dujardin, P., Fablet, A., Leroy, A., *et al*. (2024) Exploring type I interferon pathway: virulent vs. attenuated strain of African swine fever virus revealing a novel function carried by MGF505-4R. *Front. Immunol.* **15**, 1358219
94. Huang, Z., Cao, H., Zeng, F., Lin, S., Chen, J., Luo, Y., *et al*. (2023) African swine fever virus MGF505-7R interacts with interferon regulatory factor 9 to evade the type I interferon signaling pathway and promote viral replication. *J. Virol.* **97**, e01977-22
95. Li, Y., Huang, L., Weng, C., and Feng, W. (2024) ASFV pA151R negatively regulates type I IFN production via degrading E3 ligase TRAF6. *Front. Immunol.* **15**, 1339510
96. Ibrahim, N., Wicklund, A., Jamin, A., and Wiebe, M. S. (2013) Barrier to Autointegration Factor (BAF) inhibits vaccinia virus intermediate transcription in the absence of the viral B1 kinase. *Virology* **444**, 363–373
97. Wiebe, M. S., and Traktman, P. (2007) Barrier to autointegration factor is a host defense against poxvirus replication that is overcome by the viral B1 kinase. *Cell Host Microbe* **1**, 187
98. Bengtsson, L., and Wilson, K. L. (2006) Barrier-to-Autointegration factor phosphorylation on Ser-4 regulates emerin binding to lamin A in vitro and emerin localization in vivo. *Mol. Biol. Cell* **17**, 1154
99. Tang, M., Suraweera, A., Nie, X., Li, Z., Lai, P., Wells, J. W., *et al*. (2023) Mono-phosphorylation at Ser4 of barrier-to-autointegration factor (Banf1) significantly reduces its DNA binding capability by inducing critical changes in its local conformation and DNA binding surface. *Phys. Chem. Chem. Phys.* **25**, 24657–24677
100. Marcelot, A., Petitalot, A., Ropars, V., Le Du, M.-H., Samson, C., Dubois, S., *et al*. (2021) Di-phosphorylated BAF shows altered structural dynamics and binding to DNA, but interacts with its nuclear envelope partners. *Nucleic Acids Res.* **49**, 3841–3855
101. Chen, H., and Engelman, A. (1998) The barrier-to-autointegration protein is a host factor for HIV type 1 integration. *Proc. Natl. Acad. Sci.* **95**, 15270–15274
102. Broussard, G., Ni, G., Zhang, Z., Li, Q., Cano, P., Dittmer, D. P., *et al*. (2023) Barrier-to-autointegration factor 1 promotes gammaherpesvirus reactivation from latency. *Nat. Commun.* **14**, 434
103. Kobayashi, S., Koujin, T., Kojidani, T., Osakada, H., Mori, C., Hiraoka, Y., *et al*. (2015) BAF is a cytosolic DNA sensor that leads to exogenous DNA avoiding autophagy. *Proc. Natl. Acad. Sci.* **112**, 7027–7032
104. Ma, H., Qian, W., Bambouskova, M., Collins, P. L., Porter, S. I., Byrum, A. K., *et al*. (2020) Barrier-to-Autointegration factor 1 protects against a basal cGAS-STING response. *mBio* **11**, e00136-20
105. Afonso, C. L., Piccone, M. E., Zaffuto, K. M., Neilan, J., Kutish, G. F., Lu, Z., *et al*. (2004) African swine fever virus multigene family 360 and 530 genes affect host interferon response. *J. Virol.* **78**, 1858–1864
106. Gil, S., Sepúlveda, N., Albina, E., Leitão, A., and Martins, C. (2008) The low-virulent African swine fever virus (ASFV/NH/P68) induces enhanced expression and production of relevant regulatory cytokines (IFNα, TNFα and IL12p40) on porcine macrophages in comparison to the highly virulent ASFV/L60. *Arch. Virol.* **153**, 1845–1854
107. Zhang, F., Hopwood, P., Abrams, C. C., Downing, A., Murray, F., Talbot, R., *et al*. (2006) Macrophage transcriptional responses following in vitro infection with a highly virulent African swine fever virus isolate. *J. Virol.* **80**, 10514–10521
108. Zheng, X., Nie, S., and Feng, W.-H. (2022) Regulation of antiviral immune response by African swine fever virus (ASFV). *Virol. Sin.* **37**, 157–167
109. Yu, L., Zhu, Z., Deng, J., Tian, K., and Li, X. (2023) Antagonisms of ASFV towards host defense mechanisms: knowledge gaps in viral immune evasion and pathogenesis. *Viruses* **15**
110. Dixon, L. K., Islam, M., Nash, R., and Reis, A. L. (2019) African swine fever virus evasion of host defences. *Virus Res.* **266**, 25–33
111. Dupré, J., Le Potier, M.-F., Vitour, D., and Caignard, G. (2022) Modulation of the innate immune response by African swine fever virus. *Virologie* **26**, 387–400
112. Sunwoo, S.-Y., García-Belmonte, R., Walczak, M., Vigara-Astillero, G., Kim, D.-M., Szymankiewicz, K., *et al*. (2024) Deletion of MGF505-2R gene Activates the cGAS-STING pathway leading to attenuation and protection against virulent African swine fever virus. *Vaccines* **12**, 407
113. Chaudhari, J., Lai, D. C., and Vu, H. L. X. (2025) African swine fever viral proteins that inhibit cGAS-STING pathway and type-I interferon production. *Virology* **602**, 110317
114. Netherton, C. L., Connell, S., Benfield, C. T. O., and Dixon, L. K. (2019) The genetics of life and death: virus-host interactions underpinning resistance to African swine fever, a viral hemorrhagic disease. *Front. Genet.* **10**, 402

115. Elde, N. C., Child, S. J., Eickbush, M. T., Kitzman, J. O., Rogers, K. S., Shendure, J., *et al*. (2012) Poxviruses deploy genomic accordions to adapt rapidly against host antiviral defenses. *Cell* **150**, 831–841
116. Rodríguez, I., Redrejo-Rodríguez, M., Rodríguez, J. M., Alejo, A., Salas, J., and Salas, M. L. (2006) African swine fever virus pB119L protein is a flavin adenine dinucleotide-linked sulfhydryl oxidase. *J. Virol.* **80**, 3157–3166
117. Cassandri, M., Smirnov, A., Novelli, F., Pitolli, C., Agostini, M., Malewicz, M., *et al*. (2017) Zinc-finger proteins in health and disease. *Cell Death Discov.* **3**, 1–12
118. Tillo, D., Ray, S., Syed, K.-S., Gaylor, M. R., He, X., Wang, J., *et al*. (2017) The epstein-barr virus B-ZIP protein Zta recognizes specific DNA sequences containing 5-methylcytosine and 5-hydroxymethylcytosine. *Biochemistry* **56**, 6200–6210
119. García-Beato, R., Salas, M. L., Viñuela, E., and Salas, J. (1992) Role of the host cell nucleus in the replication of African swine fever virus DNA. *Virology* **188**, 637–649
120. Ballester, M., Rodríguez-Cariño, C., Pérez, M., Gallardo, C., Rodríguez, J. M., Salas, M. L., *et al*. (2011) Disruption of nuclear organization during the initial phase of African swine fever virus infection. *J. Virol.* **85**, 8263–8269
121. Margalit, A., Segura-Totten, M., Gruenbaum, Y., and Wilson, K. L. (2005) Barrier-to-autointegration factor is required to segregate and enclose chromosomes within the nuclear envelope and assemble the nuclear lamina. *Proc. Natl. Acad. Sci.* **102**, 3290–3295
122. Vizcaíno, J. A., Deutsch, E. W., Wang, R., Csordas, A., Reisinger, F., Ríos, D., *et al*. (2014) ProteomeXchange provides globally coordinated proteomics data submission and dissemination. *Nat. Biotechnol.* **32**, 223–226